AD-A149 791 DEGRADATION MECHANISMS IN CERAMIC DIELECTRICS(U) LEHIGH 1/1
UNIV BETHLEHEM PA MATERIALS RESEARCH CENTER
D M SMYTH ET AL. AUG 84 32 N00014-82-K-0190

UNCLASSIFIED F/G 9/1 NL

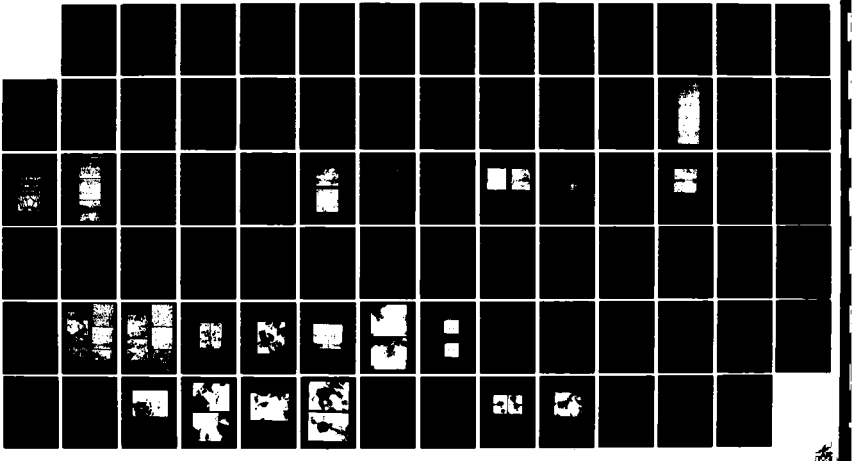

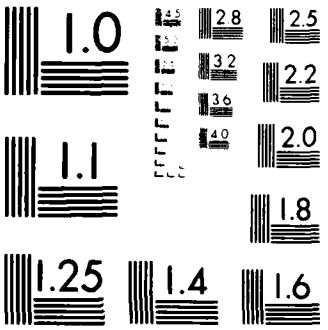

(1)

SECOND INTERIM REPORT

DEGRADATION MECHANISMS IN CERAMIC DIELECTRICS

SPONSORED BY

OFFICE OF NAVAL RESEARCH

DIVISION OF MATERIALS RESEARCH

CERAMICS PROGRAM

N00014-82-K-0190

PERIOD: May 1, 1983 - July 31, 1984

PREPARED BY: Professor D. M. Smyth
Professor M. P. Harmer
Materials Research Center, No. 32
Lehigh University
Bethlehem, PA 18015

August 1984

SECURITY CLASSIFICATION OF THIS PAGE

REPORT DOCUMENTATION PAGE

1a. REPORT SECURITY CLASSIFICATION: Unclassified	1b. RESTRICTIVE MARKINGS
2a. SECURITY CLASSIFICATION AUTHORITY	3. DISTRIBUTION/AVAILABILITY OF REPORT: DISTRIBUTION STATEMENT A Approved for public release; Distribution Unlimited
2b. DECLASSIFICATION/DOWNGRADING SCHEDULE	
4. PERFORMING ORGANIZATION REPORT NUMBER(S)	5. MONITORING ORGANIZATION REPORT NUMBER(S)
6a. NAME OF PERFORMING ORGANIZATION: Lehigh University; 6b. OFFICE SYMBOL (If applicable)	7a. NAME OF MONITORING ORGANIZATION
6c. ADDRESS (City, State and ZIP Code): Materials Research Center #32, Bethlehem, PA 18015	7b. ADDRESS (City, State and ZIP Code)
8a. NAME OF FUNDING/SPONSORING ORGANIZATION: Office of Naval Research; 8b. OFFICE SYMBOL (If applicable)	9. PROCUREMENT INSTRUMENT IDENTIFICATION NUMBER
8c. ADDRESS (City, State and ZIP Code): Division of Materials Research, Arlington, VA 22217	10. SOURCE OF FUNDING NOS. — PROGRAM ELEMENT NO. / PROJECT NO. / TASK NO. / WORK UNIT NO.
11. TITLE (Include Security Classification): Degradation in Ceramic Dielectrics (unclassified) MECHANISMS	
12. PERSONAL AUTHOR(S): Smyth, Donald M.; Harmer, Martin P.	
13a. TYPE OF REPORT: INTERIM; 13b. TIME COVERED: FROM 5/1/83 TO 7/31/84	14. DATE OF REPORT (Yr., Mo., Day): 1984, August 15; 15. PAGE COUNT
16. SUPPLEMENTARY NOTATION	
17. COSATI CODES — FIELD / GROUP / SUB. GR.	18. SUBJECT TERMS (Continue on reverse if necessary and identify by block number): Dielectric degradation; Capacitor reliability; Ceramic capacitors.

19. ABSTRACT (Continue on reverse if necessary and identify by block number)

SEE NEXT PAGE

20. DISTRIBUTION/AVAILABILITY OF ABSTRACT: UNCLASSIFIED/UNLIMITED ☒ SAME AS RPT. ☐ DTIC USERS ☐	21. ABSTRACT SECURITY CLASSIFICATION: Unclassified
22a. NAME OF RESPONSIBLE INDIVIDUAL	22b. TELEPHONE NUMBER (Include Area Code); 22c. OFFICE SYMBOL

DD FORM 1473, 83 APR EDITION OF 1 JAN 73 IS OBSOLETE

SECURITY CLASSIFICATION OF THIS PAGE

ABSTRACT

SECURITY CLASSIFICATION OF THIS PAGE

This program is designed to identify the mechanisms that lead to leakage current degradation in $BaTiO_3$-based dielectrics subjected to voltage-temperature stress, and to determine those factors that contribute to stability against such degradation. During the first year, it was confirmed that BaO-rich and donor-doped compositions are particularly stable, and that grain-size is a relatively unimportant parameter. During the second year of investigation, the microstructures of BaO-rich and donor-doped $BaTiO_3$ have been examined in detail in an effort to determine the reasons for their pronounced stability. In addition, the effect of porosity, both in amount and morphology, has been found to be an important factor.

The solubility of BaO in $BaTiO_3$ has been determined to be <100 ppm. A BaO-rich second phase corresponding to Ba_2TiO_4 was confirmed for all samples having Ba/Ti ratios $\geq$ 1.001. Thus incorporation of excess BaO by a Ruddlesden-Popper type of superlattice of the type reported for SrO-excess $SrTiO_3$ does not occur in $BaTiO_3$. The stability of BaO-rich samples is attributed to a reduction of porosity because of grain growth inhibition by the second phase. The relative instability of TiO_2-rich compositions is not related to the presence of $Ba_6Ti_{17}O_{40}$ as a second phase. This TiO_2-rich phase has been prepared and subjected to degradation tests, and has proved to be quite stable. The instability of TiO_2-rich $BaTiO_3$ is more likely due to the presence of crack-like voids.

A detailed TEM investigation of donor (niobium)-doped $BaTiO_3$ has revealed that the mode of compensation for $Nb_{Ti}^{\cdot}$ in the highly donor doped regime is by way of titanium vacancies $V_{Ti}^{''''}$ and not barium vacancies $V_{Ba}^{''}$ as previously suggested. The consequence is the formation of a titanium-rich second phase in compositions that do not have the appropriate TiO_2 deficiency. This second phase is a liquid at the firing temperature and, therefore, cannot explain the dramatic grain growth inhibition effect of Nb.

Degradation has been studied for hot pressed and sintered samples of $BaTiO_3$ with varying composition and stoichiometry. Hot pressed samples were always found to be much more stable, regardless of composition, suggesting that porosity is a major factor in degradation. Pore shape appears to be a critical factor. Electrical stability has also been found for samples exposed to strongly reducing conditions either during or after sintering. The effect is as yet unexplained.

The possibility that calcium can act as a Ti-site acceptor, $Ca_{Ti}^{''}$, has been studied further. The ALCHEMI method for determining site occupancy confirmed the presence of calcium on titanium sites for A-site excess compositions. It has also been shown that $Ca_{Ti}^{''}$ substantially lowers and broadens the ferroelectric phase transition in $BaTiO_3$, while Ca_{Ba}^{x} excess has long been known to have no such effect.

SECURITY CLASSIFICATION OF THIS PAGE

1. INTRODUCTION AND OVERVIEW

This program has focused on a study of the mechanisms of leakage current degradation in $BaTiO_3$-based ceramic dielectrics subjected to temperature-voltage stress. During the first year, it was determined that BaO-rich and donor-doped samples are particularly stable toward degradation, in general agreement with previous, unpublished results (1,2). Hot-pressed samples have recently been proved to be more stable than air-sintered material for all compositions, and this was attributed primarily to a decrease in residual porosity. In the past year, we have followed up on these clues and have determined the phase relations of the BaO-excess and donor-doped material. Studies of samples having varying amounts of porosity at constant composition have confirmed the deleterious effect of pores and has suggested that the pore shape is extremely important.

Equilibrium electrical conductivity measurements indicate that the solubility of excess BaO in $BaTiO_3$ does not exceed 100 ppm and SEM and TEM examination of the microstructure indicates that the BaO-rich second phase is Ba_2TiO_4. The solubility is insufficient to affect the concentrations of point defects significantly and the effect on degradation kinetics is more likely due to a reduction of porosity because of grain-growth inhibition by the second phase. A draft manuscript on the microstructure of BaO-rich $BaTiO_3$ is attached as Appendix A.

TEM examination of thinned donor-doped $BaTiO_3$ (6% Nb) has shown that a single-phase product is formed only for compositions corresponding to $BaTi_{1-5/4x}Nb_xO_3$. This composition has the exact Ti-deficiency required to compensate the donors with Ti vacancies, $[Nb_{Ti}^{\bullet}] = 4[V_{Ti}^{''''}]$. More Ti-rich compositions split out an excess-TiO_2 phase in order to leave the required concentration of $V_{Ti}^{''''}$ in the matrix. Thus years of speculation about

compensation by barium-vacancies and corresponding separation of BaO-rich phases proves to be incorrect. Also, the small grain size of donor-doped material cannot be due to control by the second phase, since the Ti-rich second phase, $Ba_6Ti_{17}O_{40}$, is a liquid at our sintering temperature and is known to promote grain growth. This surprising conclusion has been anticipated by recent phase studies by Jonker and Havinga (3) and by calculations of relative defect energies by Lewis and Catlow (4). A draft manuscript of our TEM work is attached as Appendix B.

Our study of the effect of porosity has confirmed that it is generally deleterious, but has also disclosed that for low pore densities the pore shape may be crucial. Elongated pores seem to be more conducive to degradation than spherical ones. Pores of predetermined distribution and shape are now being introduced. It has also been determined that pressureless sintering in the reducing atmospheres confers considerable stability. This unexpected effect is under investigation.

2. RESULTS

2.1 Effect of Porosity on Degradation

Porosity is expected to be an important factor in degradation due to the local electric field enhancement in the vicinity of a pore. To assess the importance of porosity to the degradation process a series of samples with varying degrees of porosity with fixed grain size and chemical composition have been prepared. Undoped stoichiometric samples with porosity levels ranging from 0-30 volume % were fabricated by hot pressing by terminating the pressings short of reaching full density; the final microstructures of these samples and their aging test results are shown in figures 1 and 2 respectively. As can be seen from the aging results the amount of porosity has a dramatic effect on the leakage current and degradation behavior. This can explain why hot pressed samples have been found to be far more stable than their sintered counterparts. One such example for hot pressed and sintered barium titanate (Ba/Ti = 1.000) is shown in figure 3. The only microstructural difference between the two samples is porosity as can be seen from the scanning electron micrographs shown in figure 4.

The consequences of this important result are twofold. Firstly, it impacts on the study of degradation mechanisms, especially if pressureless sintering (rather than hot pressing) is used to fabricate the test specimens. In such cases of uncontrolled porosity a high degree of caution must be exercised when interpreting degradation results. Secondly, it suggests that the search for improved ways to achieve and ensure the development of higher sintered densities (by using better sintering additives for example) promises to be a rewarding and challenging area for future research.

Further work on the effect of porosity is continuing with a study of the effects of pore shape on the degradation rate. We are currently in the

process of developing experimental methods for introducing controlled amounts of pores with variable shape (crack-like and spherical) for degradation studies.

2.2 Effect of Acceptor Doping on Degradation

Hot pressing has been used to prepare a series of fully dense samples to study the influence of acceptor doping on intrinsic degradation properties. The use of fully dense samples eliminates porosity as a factor in degradation making possible direct correlation between dopants, defect chemistry and degradation.

Initially we have studied stoichiometric barium titanate samples doped with equal amounts (1000 ppm) of either aluminum or magnesium as acceptors. Hot pressed microstructures are shown in figure 5 from which it can be seen that all samples were prepared fully dense with a uniform fine grained microstructure. The results of the aging tests are shown in figure 6 from which it can be seen that both aluminum and magnesium are effective in raising the steady state leakage events, magnesium having the more pronounced effect. In order to explain these results on the basis of the principles of defect chemistry we need to know the charge carrying species. Oxygen vacancies ($V_o^{\cdot\cdot}$) and/or holes ($h^{\cdot}$) are the two most likely charge carrier types but their relative contributions to the total conduction are not known. However, since the concentration of either defect $V_o^{\cdot\cdot}$ or $h^{\cdot}$ is predicted to increase $h^{\cdot}$ with acceptor doping, we will assume charge transport by the most widely accepted mechanism, namely that of $V_o^{\cdot\cdot}$ migration, until proved otherwise. (In a later section we will describe some future planned experiments aimed at distinguishing between $V_o^{\cdot\cdot}$ and $h^{\cdot}$ conduction.)

Assuming $V_o^{\bullet\bullet}$ conduction, then the effects of aluminum and magnesium doping on the degradation rate can be explained in terms of the influence of the respective dopants on $[V_o^{\bullet\bullet}]$. This influence can be understood on the basis of the following defect incorporation reactions for aluminum and magnesium doping respectively:

$$2BaO + Al_2O_3 \quad 2Ba_{Ba}^{x} + 5O_o^{x} + 2Al_{Ti}^{\prime} + V_o^{\bullet\bullet} \qquad (1)$$

$$[Al_{Ti}^{\prime}] = 2[V_o^{\bullet\bullet}]$$

$$BaO + MgO \rightarrow Ba_{Ba}^{x} + 2O_o^{x} + Mg_{Ti}^{\prime} + V_o^{\bullet\bullet} \qquad (2)$$

$$[Mg_{Ti}^{\prime}] = [V_o^{\bullet\bullet}]$$

The effect of both dopants can be seen to be to increase $[V_o^{\bullet\bullet}]$ which explains the higher leakage currents for these samples. The higher leakage current of the magnesium doped sample is due to its higher effective charge. Thus for equal atomic doping levels, magnesium gives twice as many $V_o^{\bullet\bullet}$ as aluminum.

The model was further examined in an experiment designed to compare the leakage currents for acceptor doped samples having the same $[V_o^{\bullet\bullet}]$ (500 ppm). (The two compositions studied were [Al] = 1000 ppm and [Mg] = 500 ppm, Ba/Ti = 1.000). As can be seen from the results (figure 7) the leakage currents for both samples were comparable consistent with the expectations of the proposed defect model. Furthermore, assuming a linear relationship between the steady state leakage current and $[V_o^{\bullet\bullet}]$ i.e. ohmic behavior (this has since been confirmed for the case of stable steady state conduction prior to degradation) it is possible to estimate the extrinsic background $[V_o^{\bullet\bullet}]$ for the undoped starting material. In our case this value was

determined (from figure 7) to be ∿50 ppm which agrees well with other published estimates (5) lending further support to the proposed defect model. The aging data of figure 7 also support the prediction (4) that defect associates such as $(Mg'_{Ti}V_O^{\cdot\cdot})$ are not important in these systems even at these very low temperatures, since the concentration of mobile $V_O^{\cdot\cdot}$ was not found to be a function of the effective charge on the acceptor.

The discussion has so far been concerned only with the results for hot pressed samples. From a practical point of view, however, we must also consider sintered materials. Here we have the added problem of separating effects due to incomplete densification (i.e. porosity) and those due to alterations in point defect concentrations. The indications are, however, that porosity is a major factor in degradation.

Aging test results comparing behavior for hot pressed and sintered samples (1000 ppm Al, Ba/Ti = 1.000) are shown in figure 8. The hot pressed sample is notably more stable with a steady state leakage current ∿3 orders of magnitude lower than that for the sintered sample. The microstructures are shown in figure 9 from which it can be seen that the only major difference between the two samples is porosity. It is argued, therefore, that porosity is the major factor contributing to the degradation of these acceptor doped sintered samples. At 4 $kVcm^{-1}$ and 100°C aluminum doped sintered samples degrade whereas undoped sintered samples tested under the same conditions do not. The aluminum doped samples have a slightly higher residual pore content and oxygen vacancy concentration in comparison to the undoped samples. We interpret this to mean that the undoped samples, due to their already high

leakage current and residual porosity, are on the verge of becoming susceptible to degradation. Further increase in pore content and $[V_O^{\cdot\cdot}]$ produced by aluminum doping, therefore, results in conditions favorable for degradation. The counter effect is demonstrated by the ability of BaO excess to restore electrical stability to aluminum doped samples by promoting the attainment of higher sintered densities. The mechanism by which BaO excess promotes densification will be discussed presently.

In summary, magnesium and aluminum as acceptor impurities in fully dense barium titanate increase the steady state leakage current consistent with a point defect model based on the creation of free unassociated oxygen vacancies. However, the dramatic differences in degradation behavior between fully dense hot pressed samples and slightly porous sintered samples indicates that porosity is still the major factor contributing to the failure of these materials by electrical degradation.

2.3 Effect of Nonstoichiometry on Degradation

(1) Ba/Ti < 1.000

It has previously been determined that pressureless sintered TiO_2-rich compositions show rapid degradation, in comparison with BaO-rich and stoichiometric compositions. The solubility of TiO_2 in $BaTiO_3$ has been estimated to be <100 ppm and, therefore, it is unreasonable to attribute the increased degradation rate of the TiO_2-rich material to a major change in defect concentration ($[V_O^{\cdot\cdot}]$).

TiO_2-rich compositions contain a second phase which has previously been identified as $Ba_6Ti_{17}O_{40}$ (6). To test if degradation can be attributed to degradation within the second phase material we have made measurements on $Ba_6Ti_{17}O_{40}$ itself. The results are shown in figure 10 from which it can be

seen that this material is extremely stable and it cannot, therefore, be held responsible for the enhanced degradation.

Degradation results for hot pressed and sintered TiO_2-excess samples are shown in figure 11. On the basis of these results and the sample microstructures (figure 12) it can be deduced that porosity is the major factor in the degradation of these materials. The difference in degradation behavior between sintered TiO_2-excess and stoichiometric samples, therefore, must be related to some difference in porosity. The final densities for TiO_2-rich samples are usually slightly higher than those for stoichiometric samples (presumably due to the beneficial effect of the liquid phase at the firing temperature in the TiO_2-excess material). Density differences alone, therefore, cannot explain the differences in behavior between these samples. Microstructural examination, however, does reveal some differences in terms of pore shapes. As can be seen from figure 13, TiO_2-excess samples contain large, sharp, crack-like voids which are not found in the stoichiometric samples. The local electric field will be enhanced more significantly at sharp crack tips such as those observed in the TiO_2-excess materials, which may explain the rapid degradation of these materials. The origin of the crack-like voids is not known and is presently under investigation.

(2) Ba/Ti > 1.000

In previous studies (7 , 2) it has been determined that BaO-excess has a stabilizing influence on the degradation properties of sintered barium titanate. The solubility of BaO in $BaTiO_3$ has been determined to be very low (<100 ppm) and Ba_2TiO_4 has been identified as the second phase present over the compositional range 1.001 < Ba/Ti < 1.100 (see attached preprint). The low solubility suggests that any explanation

based on a major change in the defect concentration ($[V_O^{\bullet\bullet}]$) can be dismissed. This leaves only porosity and the presence of Ba_2TiO_4 as a second phase as remaining factors to be considered.

Aging data for BaO-excess and stoichiometric barium titanate compositions for hot pressed and sintered samples are shown in figure 14. Several features are noteworthy from the figure: Firstly, the data show that Ba_2TiO_4 does not directly interfere with current leakage since the leakage currents for hot pressed samples with and without Ba_2TiO_4 as a second phase are the same. Secondly it demonstrates that hot pressed samples are more stable in comparison to sintered samples due to the fact that the sintered samples contain residual porosity.

Recent studies have shown that 2 mole % excess BaO promotes the sintering of barium titanate to high density (99.6%) and fine grain size (see figure 15). Having established that higher sintered density confers improved life-test performance, the higher density of the BaO-excess samples may, therefore, be the cause of the stabilizing influence of BaO-excess. The effect of BaO-excess on microstructure development is currently under study to determine the mechanism responsible for the improved microstructural evaluation. Present indications are that it is related to the grain growth inhibiting effect of the second phase Ba_2TiO_4 particles.

2.4 Calcium Doped $BaTiO_3$

We have continued with our studies on impurity site location in $BaTiO_3$ using the ALCHEMI method (Atom Location by Channeling Enhanced Microanalysis). It was concluded from ALCHEMI studies on calcium-doped $BaTiO_3$ that a definite fraction of calcium ions do occupy titanium sites (Ca''_{Ti}) in A-site-excess compositions ($\frac{Ca+Ba}{Ti} > 1$). The existence of Ca''_{Ti} has thus been directly con-

firmed. A reprint of our paper on calcium-site occupany in $BaTiO_3$ as determined by the ALCHEMI method is attached as Appendix C.

The location of calcium in the $BaTiO_3$ lattice (Ca^{x}_{Ba} or Ca''_{Ti}) has also been shown to have interesting consequences with respect to dielectric properties. It is known that Ca^{x}_{Ba} has little effect on the Curie point transition in $BaTiO_3$. However, the effect of Ca''_{Ti} on the ferroelectric phase transition in $BaTiO_3$ has nto previously been determined and therefore a study was initiated. Dielectric measurements were conducted at the National Center for Dielectric Studies at Pennsylvania State University. Figure 16 shows the effect of Ca''_{Ti} on the Curie point transition for $[Ca''_{Ti}]$= 1 and 2 atom %. It can be seen from the figure that Ca''_{Ti} substantially lowers and broadens the Curie-point transition in $BaTiO_3$. The cause of this interesting effect and its implications to commercial capacitor manufacture are being considered.

Studies on the effect of Ca''_{Ti} on degradation have continued. Pressureless sintered samples show a trend of increasing degradation rate with increasing $[Ca''_{Ti}]$ (figure 17). It is tempting to relate the enhancement in degradation to a corresponding increase in $[V_o^{\cdot\cdot}]$ due to Ca''_{Ti} doping. However, microstructure may also be a factor since all of these compositions become stable when hot pressed (figure 18).

2.5 Microstructure of Donor Doped $BaTiO_3$

While small additions of donor impurities are compensated by electrons that result from oxygen loss

$$Nb_2O_5 + 2BaO \rightarrow 2Nb^{\cdot}_{Ti} + 2Ba_{Ba} + 6O_o + 1/2O_2 + 2e' \qquad (3)$$

it is known that for additions >0.5 mol % there is no oxygen loss and the resulting material is a good insulator

$$Nb_2O_5 + 2BaO \rightarrow 2Nb_{Ti}^{\bullet} + 2Ba_{Ba} + 6O_o + O_?^{''} \quad (4)$$

where $O_?^{''}$ indicates ignorance about the mode of incorporation of the crystallographic excess of oxygen (3). Recent work by Jonker and Havinga (3) claimed that single phase material results only for the composition $BaTi_{1-5/4x}Nb_xO_3$ which implies compensation of the donors by $V_{Ti}^{''''}$

$$2Nb_2O_5 + 5BaO \rightarrow 4Nb_{Ti}^{\bullet} + 5Ba_{Ba} + V_{Ti}^{''''} + 15O_o \quad (5)$$

we have prepared samples having the compositions $Ba_{1-x/2}Ti_{1-x}Nb_xO_3$, $BaTi_{1-x}Nb_xO_{3+x/2}$, and $BaTi_{1-5/4x}Nb_xO_3$. The first has just the right amount of missing Ba to compensate the $Nb_{Ti}^{\bullet}$ with $V_{Ba}^{''}$

$$Nb_2O_5 + BaO \rightarrow 2Nb_{Ti}^{\bullet} + Ba_{Ba} + V_{Ba}^{''} + 6O_o \quad (6)$$

while the second composition corresponds to filled cation sublattices with Ba/(Ti+Nb)=1.000. Examination of thinned samples by TEM disclosed a Ti-rich second phase in the first two compositions. but there was no second phase in the third. Thus the material will always split out a Ti-rich second phase, presumably $Ba_6Ti_{17}O_{40}$ (6), as necessary to leave just enough $V_{Ti}^{''''}$ to compensate the donor impurities (see Appendix B). This is in accord with recent calcualtions of defect energetics in $BaTiO_3$ that indicated that $V_{Ti}^{''''}$ is energetically more favorable than $2V_{Ba}^{''}$ (4). It also confirms the observations of Jonker and Havinga.

A major factor contributing to the excellent stability of these highly donor doped materials is undoubtedly the much reduced $V_o^{\bullet\bullet}$ content. Other factors may be the presence of a stable titania-rich second phase and an improved microstructure due to the grain growth inhibiting effect of the donor. The relative importance of these separate contributions is under study, as is the mechanism responsible for the grain growth inhibition.

2.6 Effect of Sintering Atmosphere

In order to obtain fully dense samples with small grain size, hot-pressing has been used. It was soon noted that all such samples showed a high level of stability against degradation, regardless of composition. This has been attributed entirely to the lack of porosity, and that is undoubtedly a factor, but another factor must also be considered. Up to the present time, the hot-pressing has been carried out in an atmosphere exposed to graphite heating elements. In one resistance heated unit the atmosphere is nitrogen gas, while in an RF heated furnace the working space is evacuated by means of a mechanical pump. In both cases the oxygen activity must be very low because the gas is exposed to the hot graphite elements. In order to check the effect of this exposure to reducing conditions, sintering without application of pressure was carried out in the same equipment. Again, the samples proved to be quite stable (see figure 19).

After densification in a reducing atmosphere, the samples must be reoxidized to an insulating state before being subjected to the degradation test. It was found that adequate reoxidation required 10-20 hours in air in the vicinity of 1000°C, much longer than expected from our experience with equilibration times during measurements of the equilibrium electrical conductivity. Such sluggish reoxidation behavior has previously been observed after reduction in CO/CO_2 mixtures so rich in CO as to be unstable with regard to disproportionation resulting in carbon deposition

$$2CO \rightarrow CO_2 + C \qquad (7)$$

Carbon deposits throughout the sample and is reoxidized only very slowly. In the densification studies, an oxygen-poor atmosphere is in contact with the hot graphite elements. There it can react to give a local mixture of $CO-CO_2-O_2$ approximating the equilibrium composition in contact with solid carbon. Carbon

deposition is favored at lower temperatures and the $BaTiO_3$ samples are not as hot as the surface of the heating elements. Therefore the gas mixture generated at the element is unstable at the surface of the samples and carbon is continuously transported from element to sample. Clearly we need to redo these studies with a controlled gas composition not in contact with carbon.

In any case, the peculiar stability of these samples is of great interest, and the reasons for it are not yet apparent. One additional clue was obtained in an experiment in which a sample was sintered in air and then put through the pressureless sintering cycle in the hot press atmosphere and reoxidized. Its stability was equivalent to that of samples sintered in the reducing atmosphere in the first place. It is essential to determine whether the critical factor is the carbon, a difference in porosity, or some other unknown aspect of exposure to the reducing atmosphere.

3. FUTURE PLANS

In the remaining several months prior to the expiration of the current contract period we plan to complete our studies on the microstructure development and degradation of BaO-excess $BaTiO_3$. We will continue studying the effects of pore shape, donor doping and reduced atmosphere sintering, although we anticipate that the completion of this work will take us into a new contract period for which a renewal proposal is presently being prepared. A major thrust of the renewal proposal will be the identification of the charge carrier type (oxygen vacancies or holes) through a series of carefully planned experiments which will enable us to study the effects of varying $[V_O^{\bullet\bullet}]$ at constant $[h^{\bullet}]$ and vice versa. These data will be further supplemented by direct transport number measurement.

REFERENCES

1. A. Gruver, et al., "State of the Art Review on Ferroelectric Ceramic Materials," Tech. Report AFML-RT-66-164, Linden Laboratories, Inc., State College, Pennsylvania (1966).

2. J. D. Keck, Tehsis, University of Missouri-Rolla (1976).

3. G. H. Jonker and E. E. Havinga, "The Influence of Foreign Ions on the Crystal Lattice of Barium Titanate," Mat. Res. Bull.; 17, 345-350 (1982).

4. G. V. Lewis and C. R. A. Catlow, "Computer Modelling of Barium Titanate," Radiation Effects, 73, 307-314 (1983).

5. N. H. Chan, R. K. Sharma, and D. M. Smyth, "Nonstoichiometry in Acceptor-Doped $BaTiO_3$," J. Am. Ceram. Soc., 65[3], 167-70 (1982).

6. R. K. Sharma, N. H. Chan and D. M. Smyth, "Solubility of TiO_2 in $BaTiO_3$," J. Am. Ceram. Soc., 64[8], 448-51 (1981).

7. D. M. Smyth and M. P. Harmer, "Degradation Mechanisms in Ceramic Dielectrics," First Interim Report to Office of Naval Research N00014-82-K-0190.

8. N. G. Eror and D. M. Smyth, "Oxygen Stoichiometry of Donor-Doped $BaTiO_3$ and TiO_2," pp. 62-74 in The Chemistry of Extended Defects in Non-Metallic Solids, L. Eyring and M. O'Keefe, Editors, North Holland, Amsterdam (1970).

PERSONNEL

Professor D. M. Smyth, Principal Investigator

Professor M. P. Harmer, Faculty Associate

Dr. Helen Chan, Research Associate

Dr. Misri Lal, Research Associate

Mr. Yung Haw-Hu, Ph.D. Candidate

Mr. Albert Valentino, Ph.D. Candidate

PUBLICATIONS

The effects of composition and microstructure on electrical degradation in $BaTiO_3$, M. P. Harmer, Y. H. Hu, M. Lal, and D. M. Smyth, Ferroelectrics 49, 71-74 (1983).

Resistance degradation in ceramic capacitors, M. P. Harmer and D. M. Smyth, Proc. of the 4th Intern. Conf. in Reliability and Maintainability, May 21-25 (1984), 132-6, Perros-Guirec.

Calcium site occupancy in $BaTiO_3$, H. M. Chan, M.P. Harmer, M. Lal, and D. M. Smyth, Proc. of the Symp. on Electron Microscopy of Materials, Materials Research Society, in press.

Solubility of BaO in $BaTiO_3$, Y.H. Hu, M. P. Harmer and D. M. Smyth, submitted to J. Am. Ceram. Sco, August (1984).

PRESENTATIONS

Electrical degradation of $BaTiO_3$, M. Lal and D. M. Smyth, Paper 29-E-83, 85th Annual Meeting of the American Ceramic Society, April 26, 1983, Chicago

The effects of composition and microstructure on electrical degradation in $BaTiO_3$, M. P. Harmer, Y. H. Hu, M. Lal, and D. M. Smyth, 1983 IEEE International Symposium on Applications of Ferroelectrics, June 1, 1983, Gaithersburg, MD.

The effect of microstructure on electrical degradation of dielectrics based on $BaTiO_3$, M. P. Harmer, Y. H. Hu, M. Lal, and D. M. Smyth, Paper 25-E-83F, Electronics Divsiion Meeting, American Ceramic Society, September 13, 1983, Grossinger's, NY.

Calcium site occupancy in $BaTiO_3$, H. M. Chan, M. P. Harmer, M. Lal, and D. M. Smyth, 1983 Annual Meeting of the Materials Research Society, November 16, 1983, Boston.

Electron microscopy studies of Nb-doped $BaTiO_3$, H. Chan, M. P. Harmer, and D. M. Smyth, Paper 50-E-84, 86th Annual Meeting of the American Ceramic Society, May 1, 1984, Pittsburgh.

Electrical degradation of fully dense undoped and acceptor doped $BaTiO_3$, Y. H. Hu, M. P. Harmer, and D. M. Smyth, Paper 70-E-84, 86th Annual Meeting of the American Ceramic Society, May 1, 1984, Pittsburgh.

Electrical degradation of Ca-doped $BaTiO_3$, M. Lal, M. P. Harmer, and D. M. Smyth, Paper 71-E-84, 86th Annual Meeting of the American Ceramic Society, May 1, 1984, Pittsburgh.

Compensation of donor-impurities in $BaTiO_3$ by calcium, Y. Sakabe, J. Appleby, Y. H. Han, D. Wintergrass, and D. M. Smyth, Paper 123-E-84, 86th Annual Meeting of the American Ceramic Society, May 3, 1984, Pittsburgh.

Resistance degradation in ceramic capacitors, M. P. Harmer and D. M. Smyth 4th International Conference on Reliability and Maintainability, May 23, 1984, Perros-Guirec, France.

Solubility of BaO in $BaTiO_3$, Y. H. Hu, M. P. Harmer, and D. M. Smyth, to be presented at the Electrons Division Meeting, American Ceramic Society, October 29, 1984, San Francisco.

Effect of calcium on the ferroelectric transition in $BaTiO_3$, M. Lal, Y. H. Hu, M. P. Harmer, and D. M. Smyth, to be presented at the Electrons Division Meeting, American Ceramic Society, October 30, 1984, San Francisco.

The effects of pore density and morphology on electrical degradation of $BaTiO_3$ Y. H. Hu, M. Lal, M. P. Harmer, and D. M. Smyth, to be presented at the Electrons Division Meeting, American Ceramic Society, October 30, 1984, San Francisco.

Foreign Travel

Professor Smyth attended the Fourth International Conference on Reliability, May 21-25, 1984, in Perros-Guirec, France, and offered a technical contribution entitled "Resistance Degradation in Ceramic Dielectrics", coauthored with Professor Harmer. Visits to universities and laboratories were also arranged, and included the following:

Centre de Recherches sur la Physique des Hautes Temperatures (CNRS), Orleans, Drs. Cales and Odier.

Laboratoire de Physique Electronique et Thermodynamique des Oxydes, University of Tours, Professors Lecomte and Loup.

Laboratoire de Cristallographic Chimie et Physique du Solide, University of Caen, Professors Desgardin and Raveau.

CNET Lannion B (Centre National d'Etudes des Telecommunications) Dr. Hansonne.

Details of the visits and of the conference are included in a separate trip report.

FIGURE CAPTIONS

Figure 1. Hot pressed microstructures for undoped $BaTiO_3$ samples hot pressed to different densities; 70%, 89% and 96%.

Figure 2. The effect of porosity on degradation behavior for hot pressed undoped $BaTiO_3$.

Figure 3. Degradation tests for hot pressed and sintered undoped $BaTiO_3$.

Figure 4. Microstructures of hot pressed (A) and sintered (B) undoped $BaTiO_3$.

Figure 5. Microstructures for hot pressed undoped (A), 1000 ppm Al doped (B) and 1000 ppm Mg doped (C) stoichiometric $BaTiO_3$.

Figure 6. Degradation data for undoped, 1000 ppm Al doped and 1000 ppm Mg doped hot pressed $BaTiO_3$.

Figure 7. Degradation data for undoped, 1000 ppm Al doped and 500 ppm Mg doped hot pressed $BaTiO_3$.

Figure 8. Degradation data for hot pressed and sintered $BaTiO_3$ containing 1000 ppm Al, Ba/Ti = 1.000.

Figure 9. Microstructures for hot pressed (A) and sintered (B) $BaTiO_3$ containing 1000 ppm Al, Ba/Ti = 1.000.

Figure 10. Degradation data for sintered $Ba_6Ti_{17}O_{40}$ and TiO_2-excess $BaTiO_3$.

Figure 11. Degradation data for hot pressed and sintered TiO_2-excess $BaTiO_3$.

Figure 12. Microstructures for hot pressed (A) and sintered (B) TiO_2-excess $BaTiO_3$.

Figure 13. Microstructures for stoichiometric (A) and TiO_2-excess (B) sintered $BaTiO_3$.

Figure 14. Degradation data for stoichiometric and BaO-excess $BaTiO_3$, hot pressed and sintered.

Figure 15. Microstructure of sintered BaO-excess $BaTiO_3$, Ba/Ti=1.02.

Figure 16. Effect of Ca''_{Ti} on the Curie point transition for calcium-doped $BaTiO_3$.

Figure 17. Effect of Ca''_{Ti} content on degradation for sintered $BaTiO_3$.

Figure 18. Degradation rate for hot pressed and sintered calcium-doped $BaTiO_3$.

Figure 19. Effect of sintering atmosphere on degradation rate for calcium-doped $BaTiO_3$.

Ba/Ti = 1.000

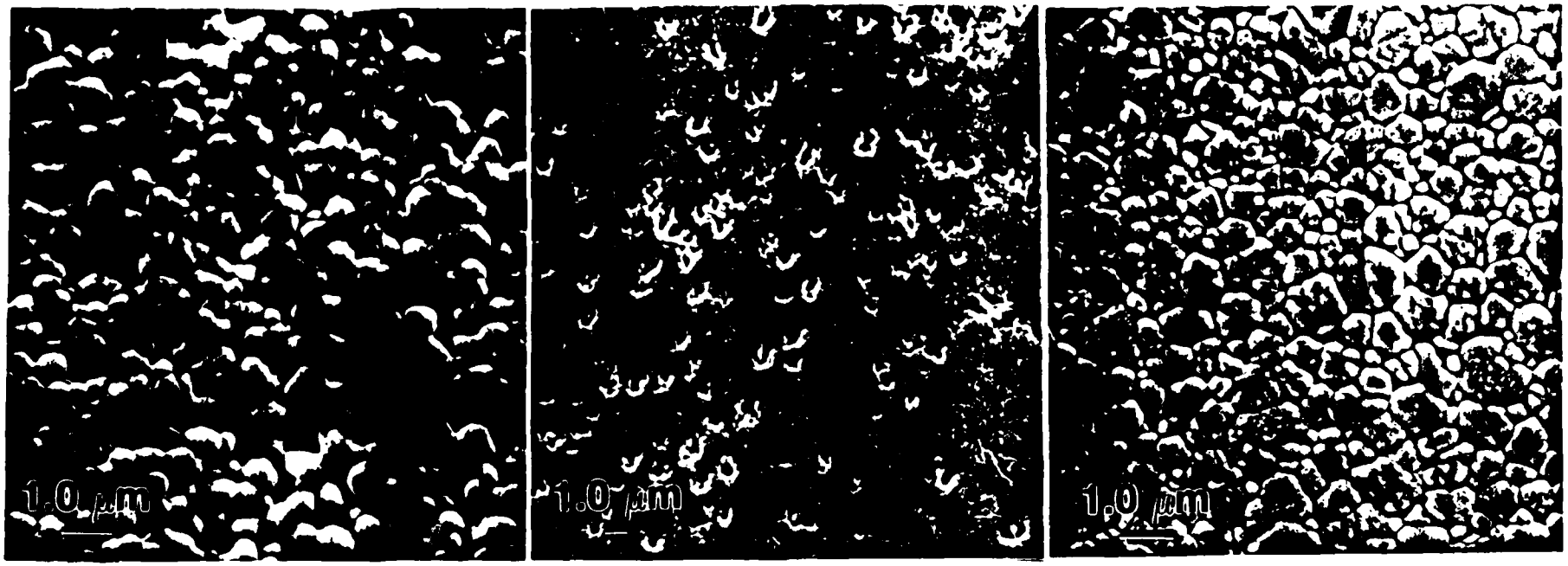

70 %

89 %

96 %

Figure 1.

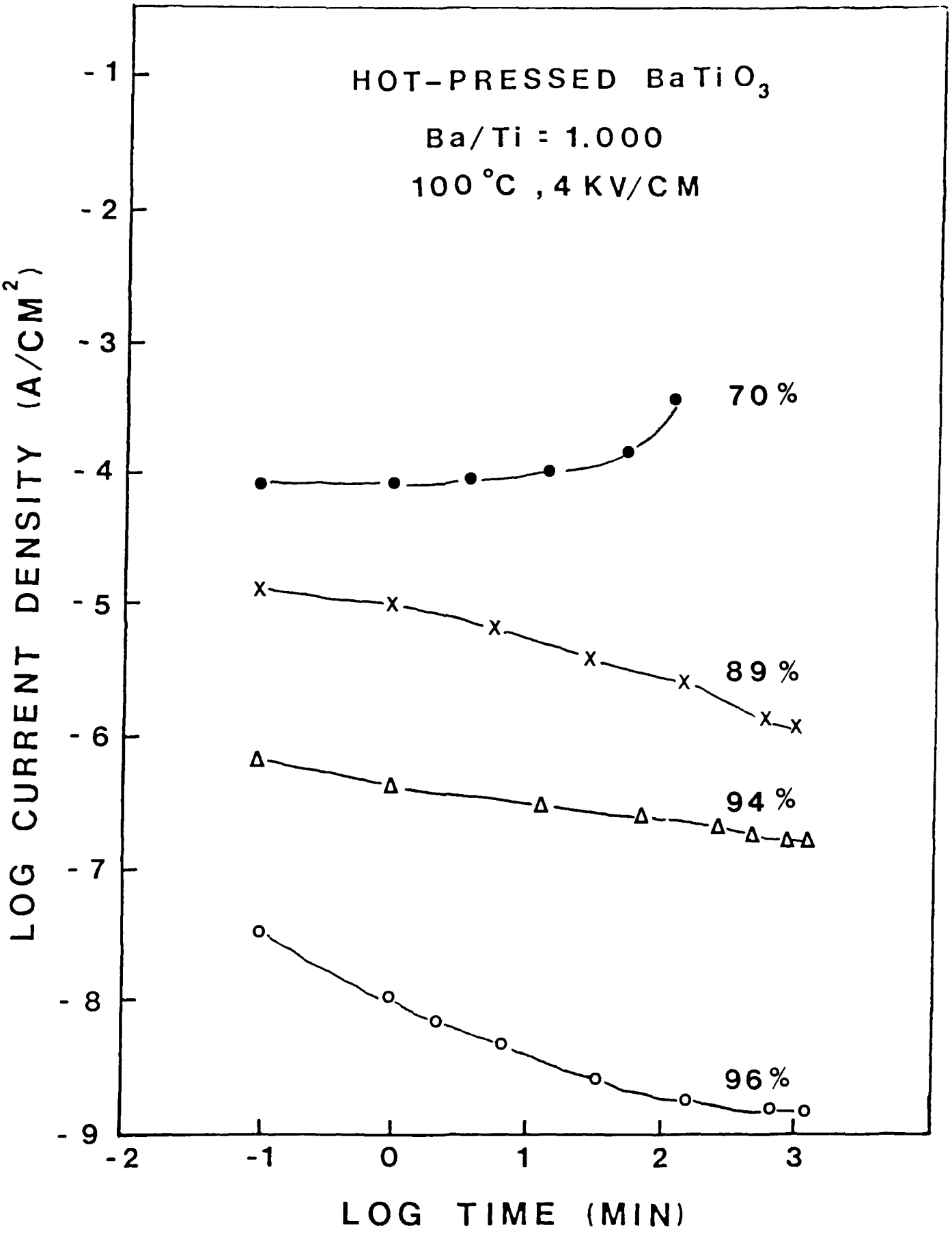
HOT-PRESSED BaTiO3
Ba/Ti = 1.000
100 °C , 4 KV/CM
70 %
89 %
94 %
96 %
LOG CURRENT DENSITY (A/CM2)
LOG TIME (MIN)
-1
-2
-3
-4
-5
-6
-7
-8
-9
-2
-1
0
1
2
3

Figure 2.

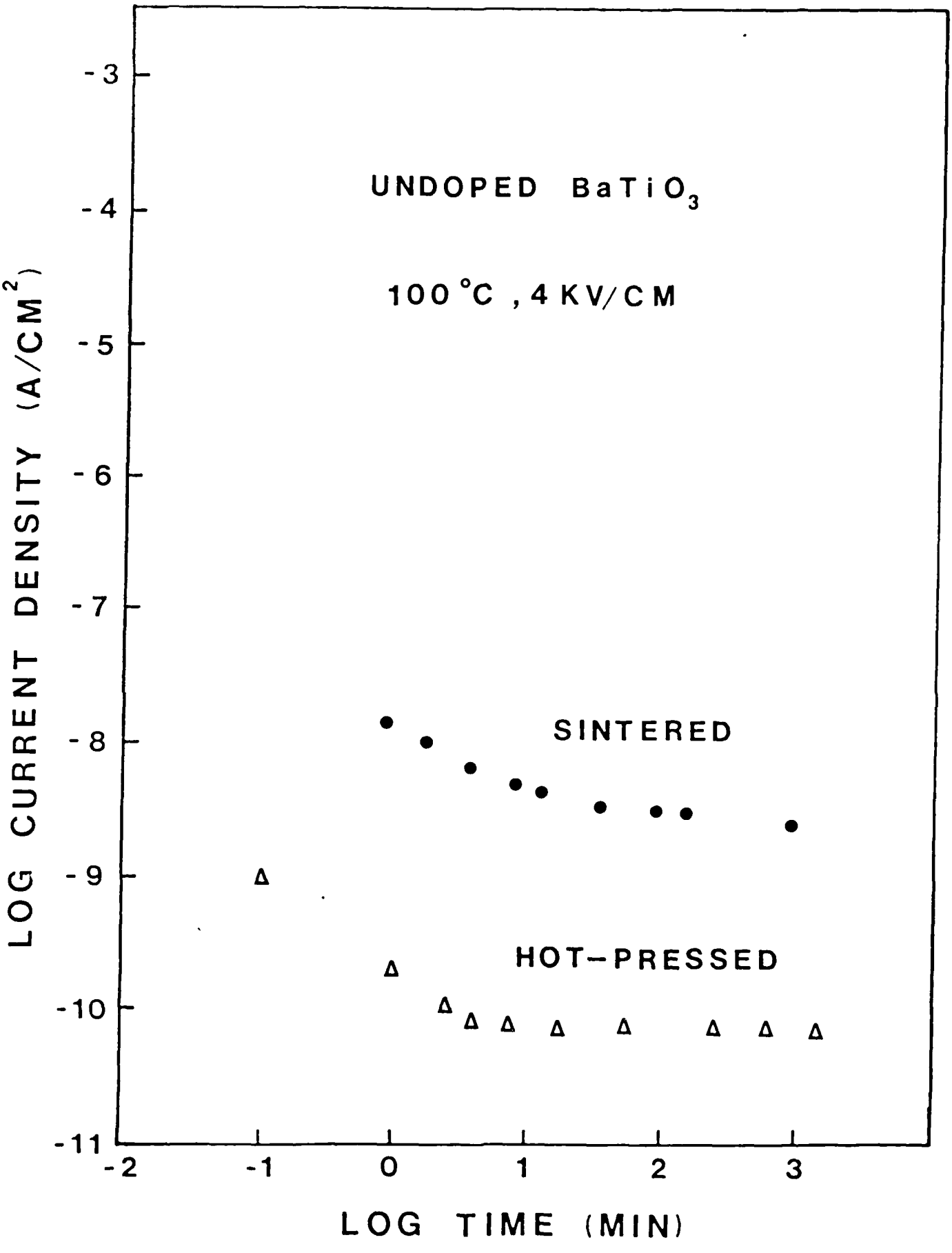
UNDOPED $BaTiO_3$
100 °C , 4 KV/CM
SINTERED
HOT-PRESSED
LOG CURRENT DENSITY (A/CM^2)
LOG TIME (MIN)
-3
-4
-5
-6
-7
-8
-9
-10
-11
-2
-1
0
1
2
3

Figure 3.

UNDOPED

HOT-PRESSED

SINTERED

Figure 4.

A/B = 1.000

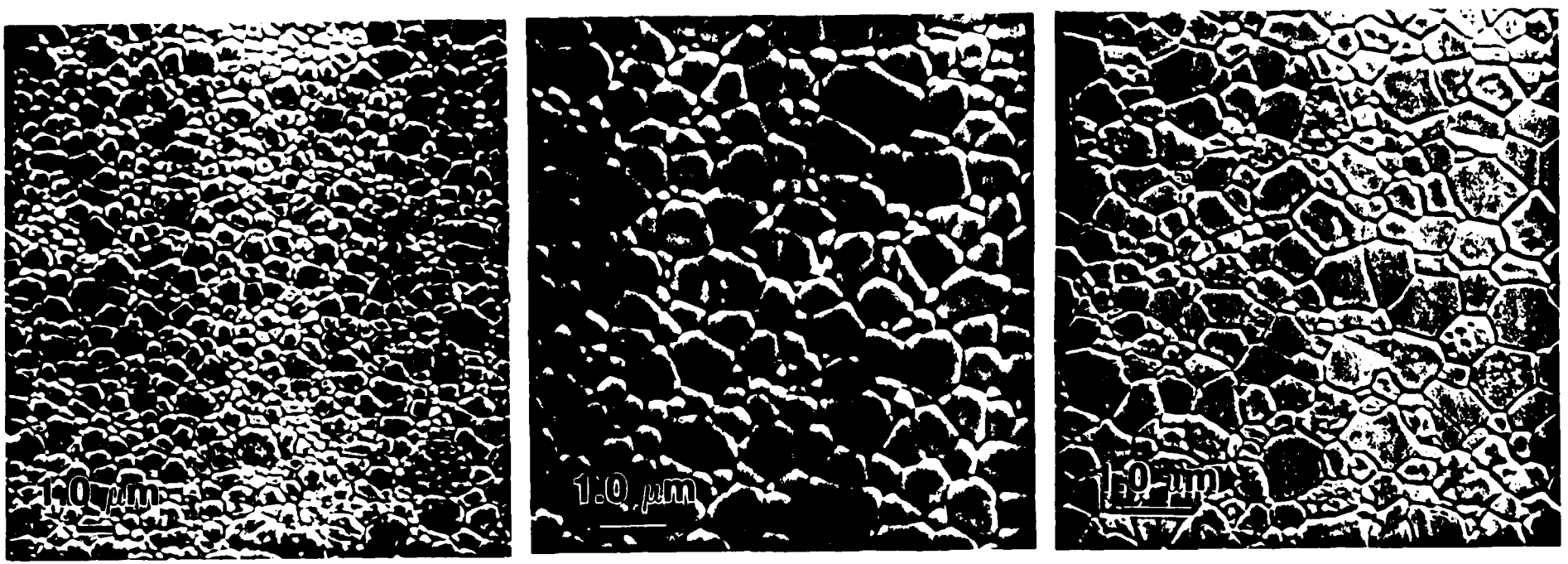

UNDOPED

1000 ppm Al

1000 ppm Mg

Figure 5.

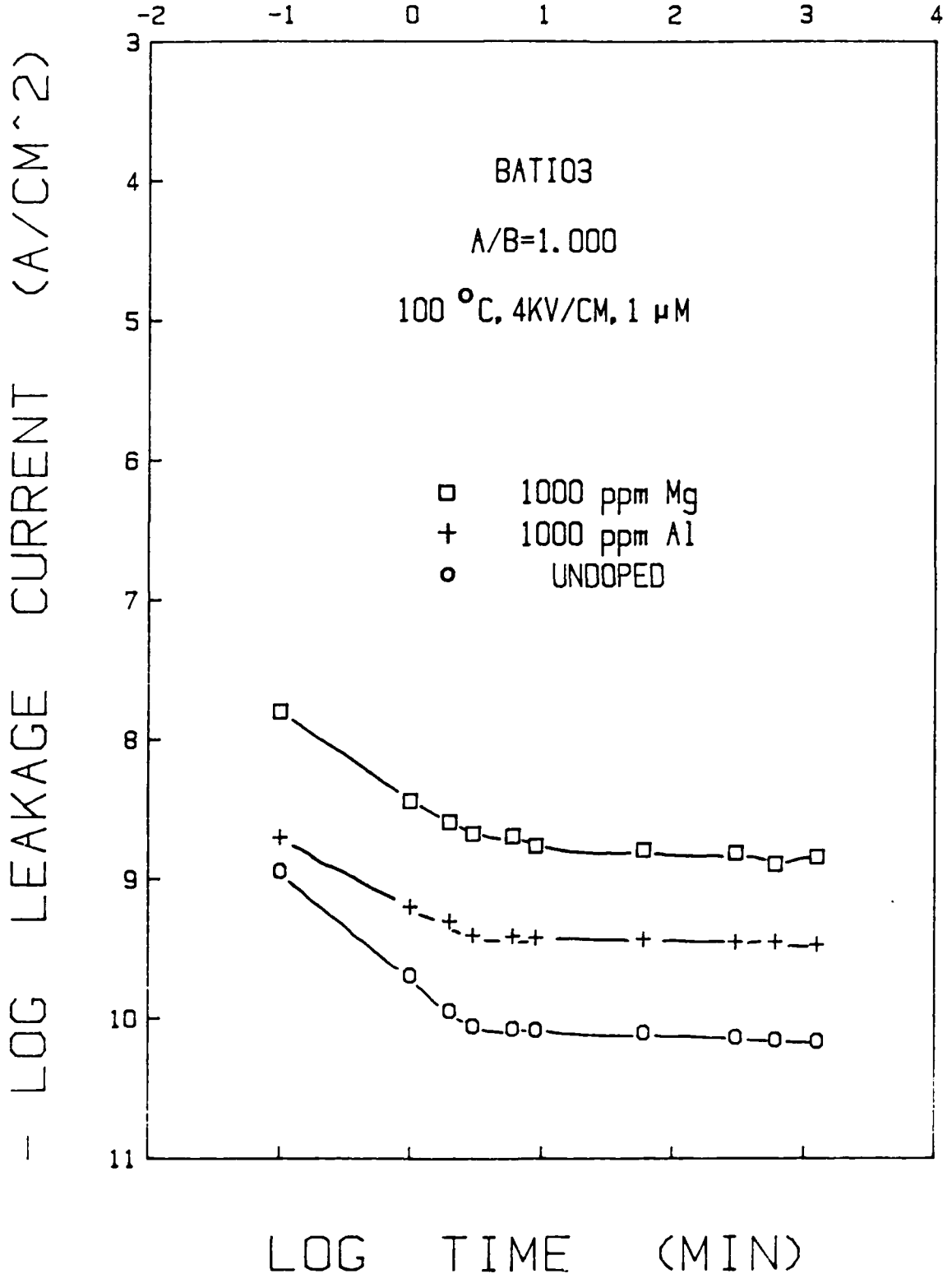
-2
-1
0
1
2
3
4
3
4
5
6
7
8
9
10
11
BATIO3
A/B=1.000
100 °C, 4KV/CM, 1 μM
1000 ppm Mg
1000 ppm Al
UNDOPED
- LOG LEAKAGE CURRENT (A/CM^2)
LOG TIME (MIN)

Figure 6.

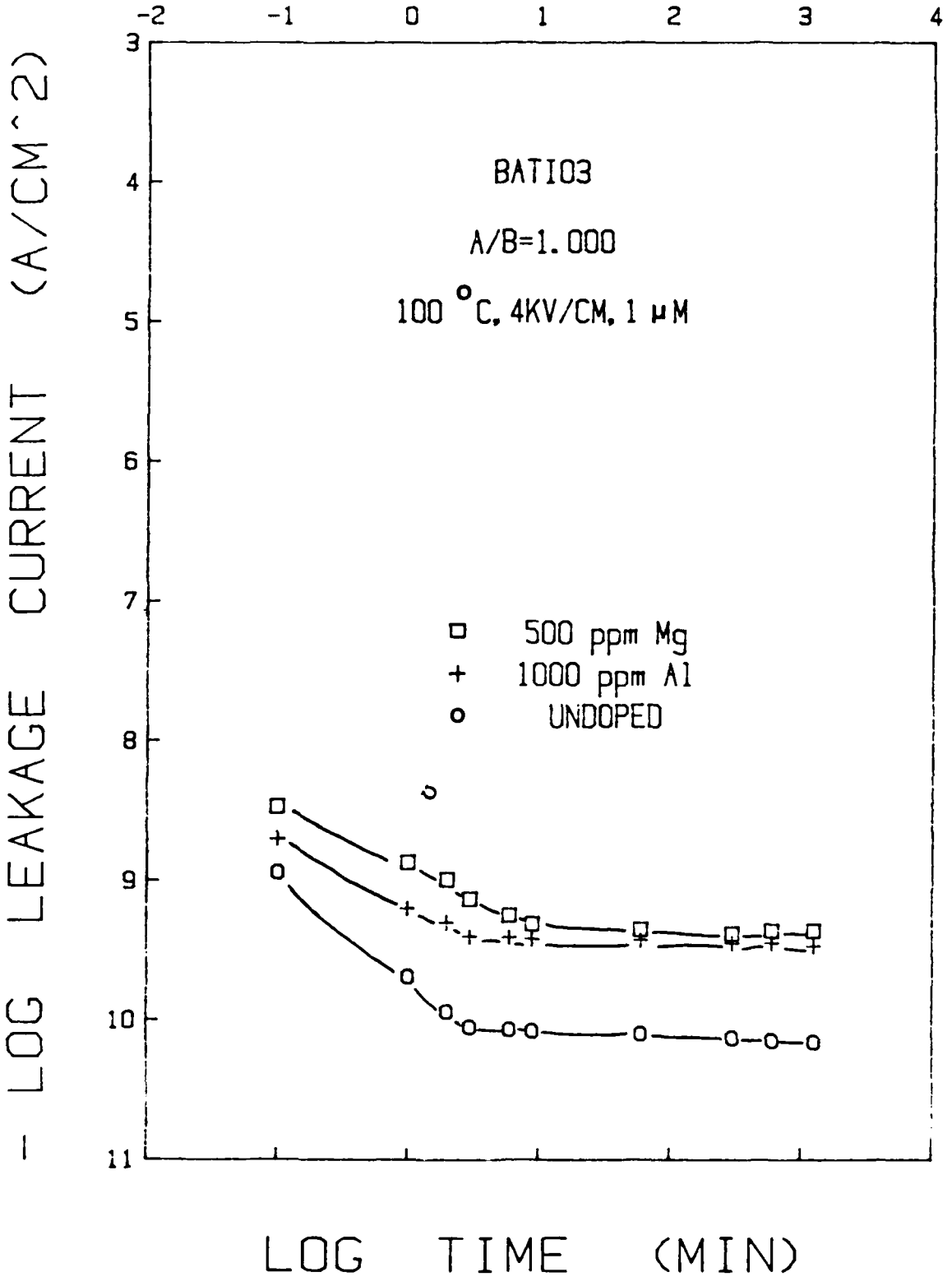
-2
-1
0
1
2
3
4
3
4
5
6
7
8
9
10
11
BATIO3
A/B=1.000
100 °C, 4KV/CM, 1 μM
500 ppm Mg
1000 ppm Al
UNDOPED
- LOG LEAKAGE CURRENT (A/CM^2)
LOG TIME (MIN)

Figure 7.

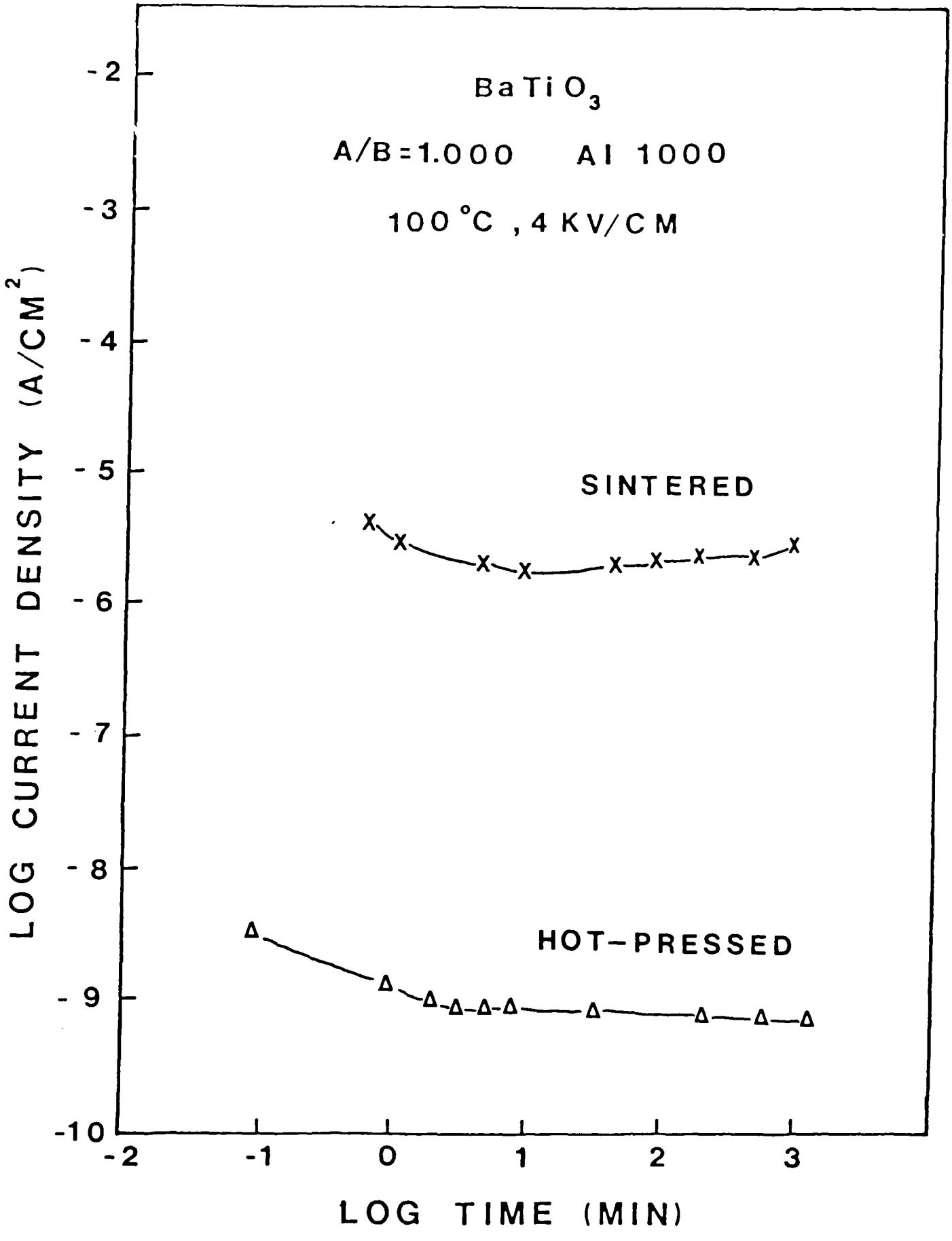
BaTiO3
A/B=1.000 Al 1000
100°C, 4 KV/CM
SINTERED
HOT-PRESSED
LOG CURRENT DENSITY (A/CM2)
LOG TIME (MIN)
-2
-3
-4
-5
-6
-7
-8
-9
-10
-2
-1
0
1
2
3

Figure 8.

1000 ppm Al

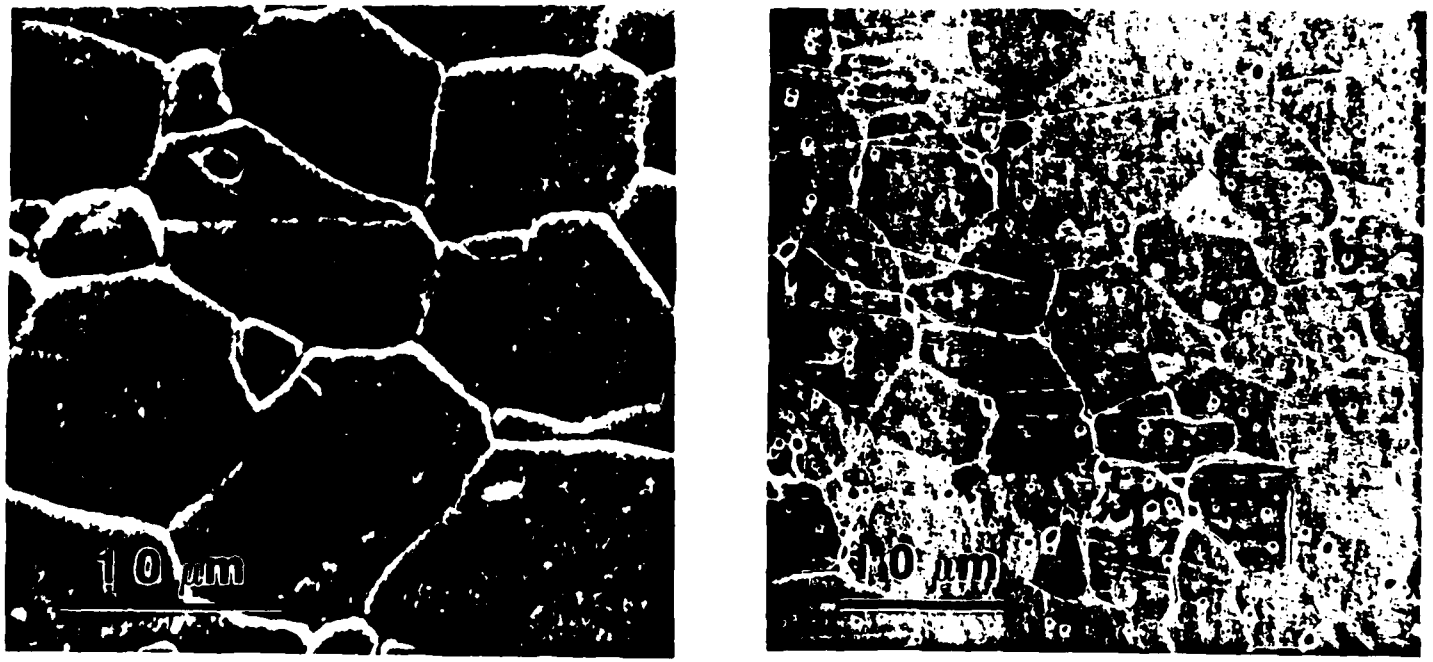

HOT-PRESSED

SINTERED

Figure 9.

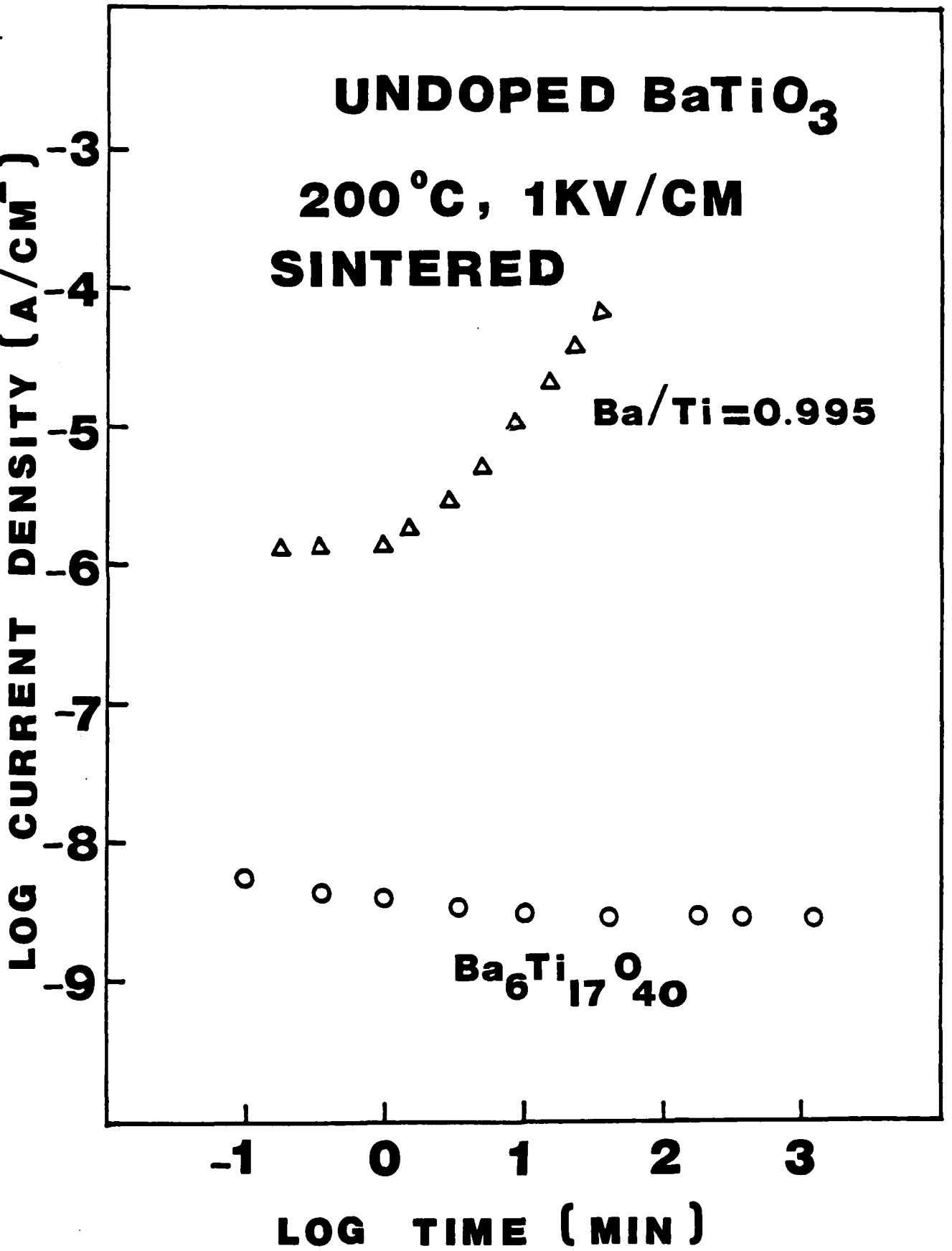
UNDOPED BaTiO3
200°C, 1KV/CM
SINTERED
Ba/Ti=0.995
Ba6Ti17O40
LOG CURRENT DENSITY (A/CM2)
-3
-4
-5
-6
-7
-8
-9
-1
0
1
2
3
LOG TIME (MIN)

Figure 10.

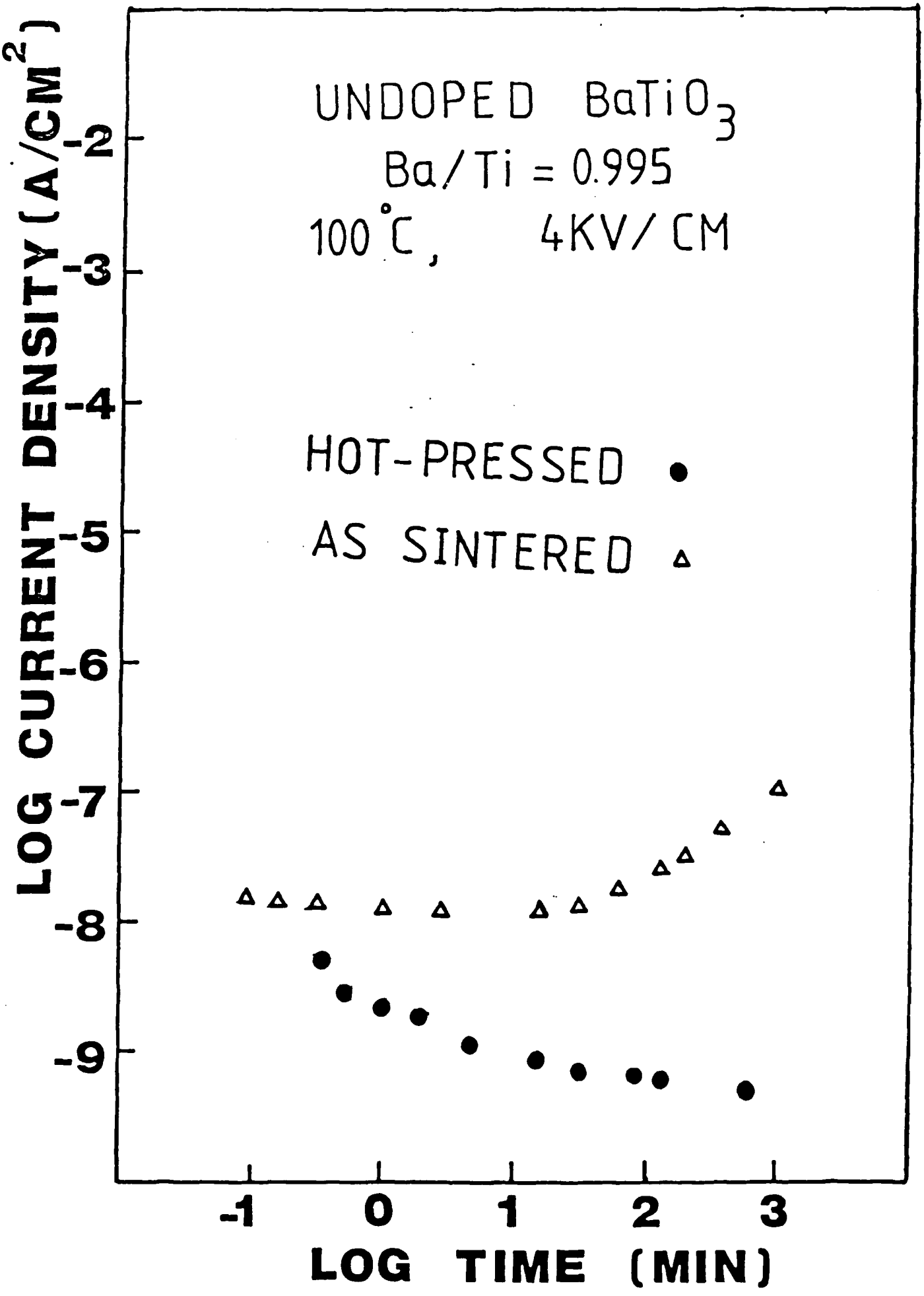
UNDOPED $BaTiO_3$
Ba/Ti = 0.995
100°C, 4KV/CM
HOT-PRESSED
AS SINTERED
LOG CURRENT DENSITY (A/CM^2)
-2
-3
-4
-5
-6
-7
-8
-9
-1
0
1
2
3
LOG TIME (MIN)

Figure 11.

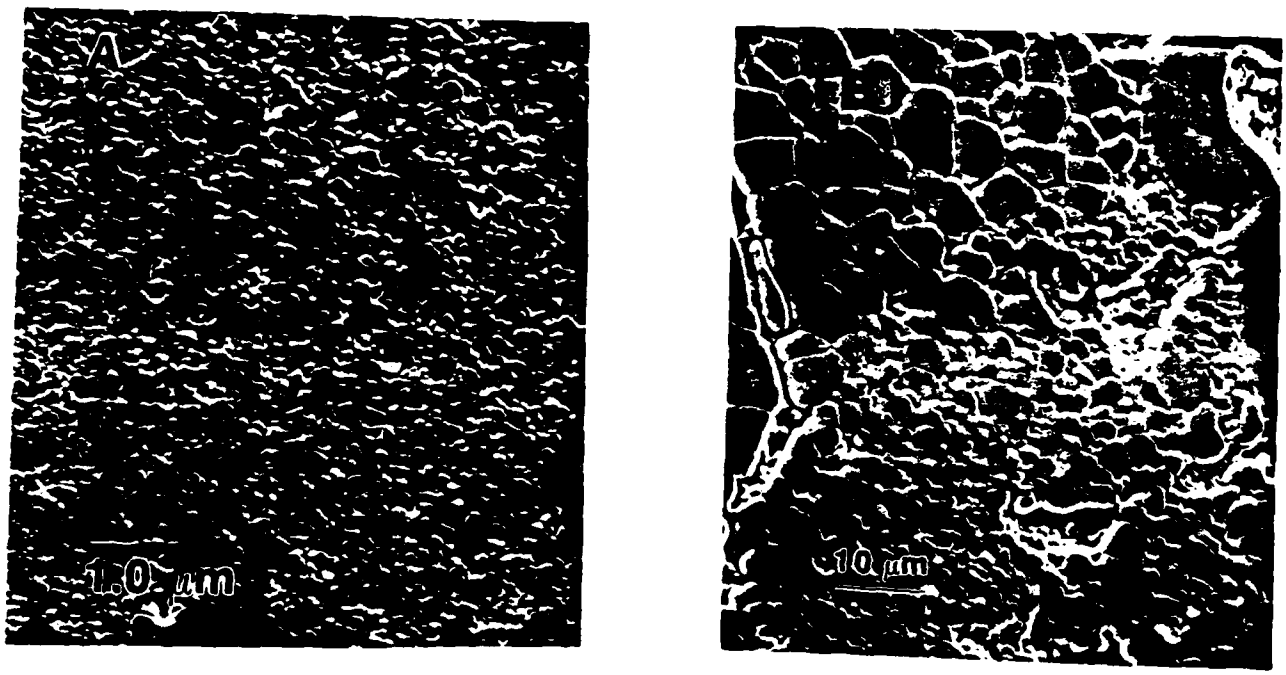

Figure 12.

STOICHIOMETRIC (Ba/Ti = 1.000)

TiO_2 EXCESS (Ba/Ti = 0.995)

Figure 13.

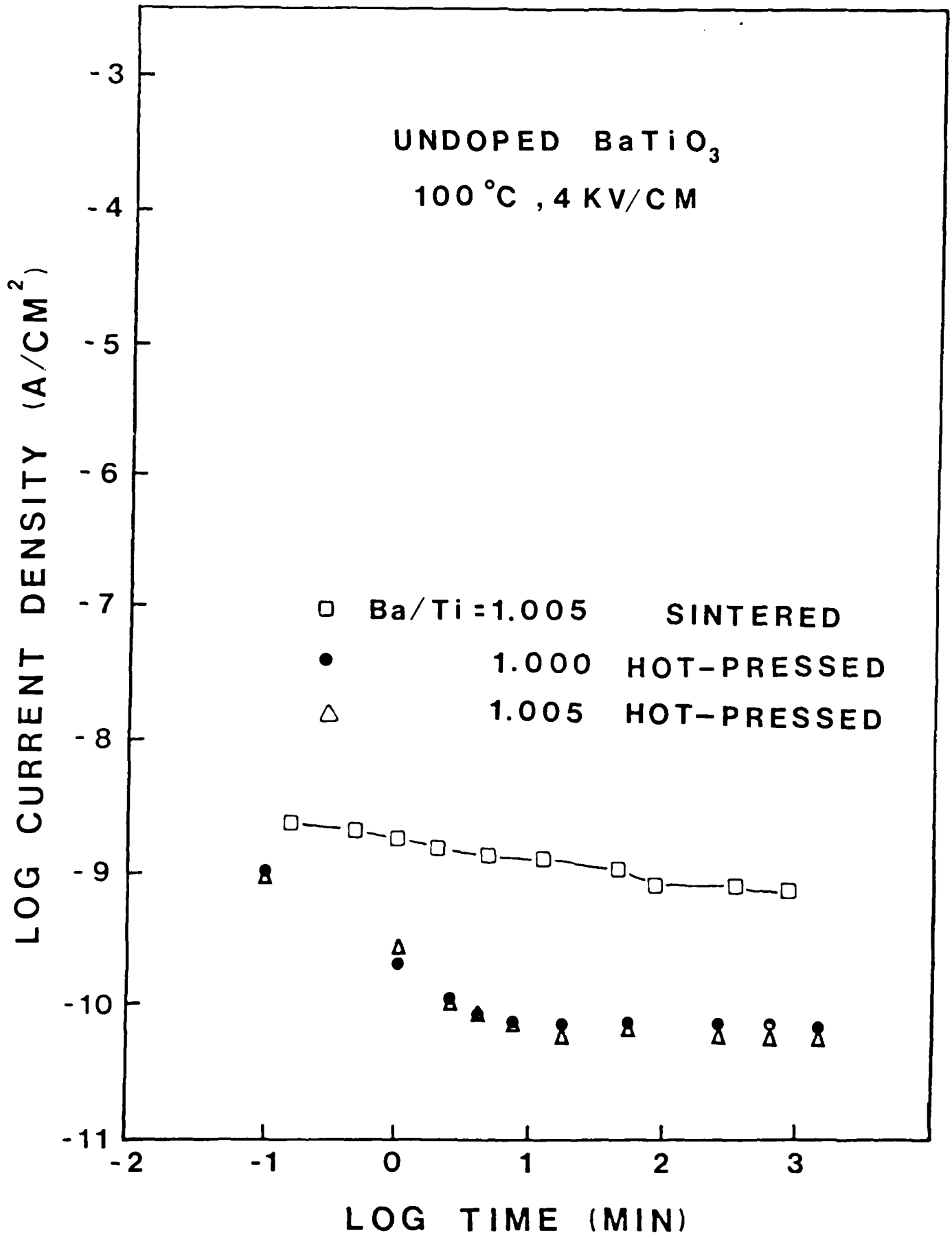
UNDOPED $BaTiO_3$
100 °C , 4 KV/CM
Ba/Ti = 1.005 SINTERED
1.000 HOT-PRESSED
1.005 HOT-PRESSED
LOG CURRENT DENSITY (A/CM^2)
LOG TIME (MIN)
-3
-4
-5
-6
-7
-8
-9
-10
-11
-2
-1
0
1
2
3

Figure 14.

Figure 15.

AIR SINTERED

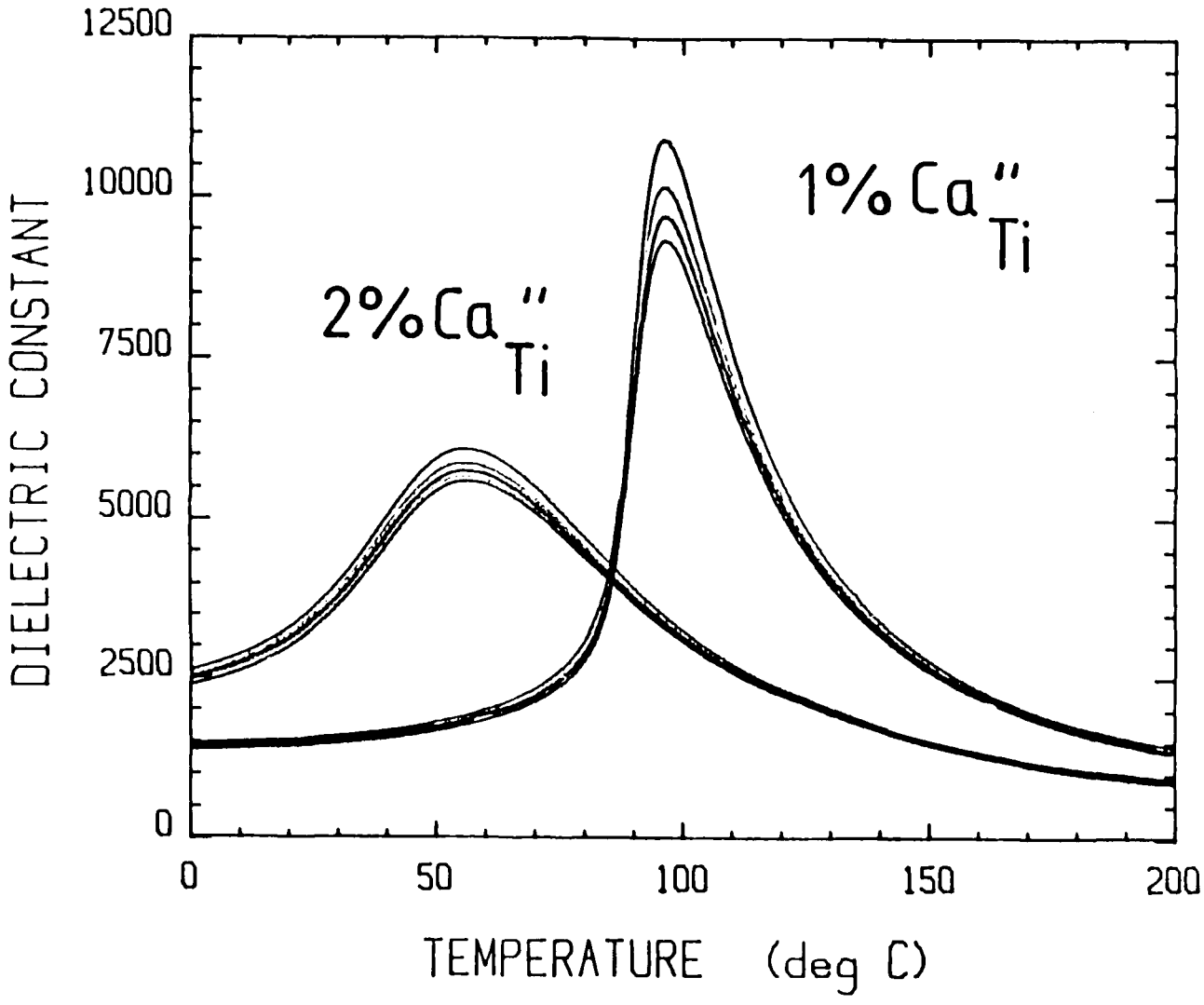

Figure 16.

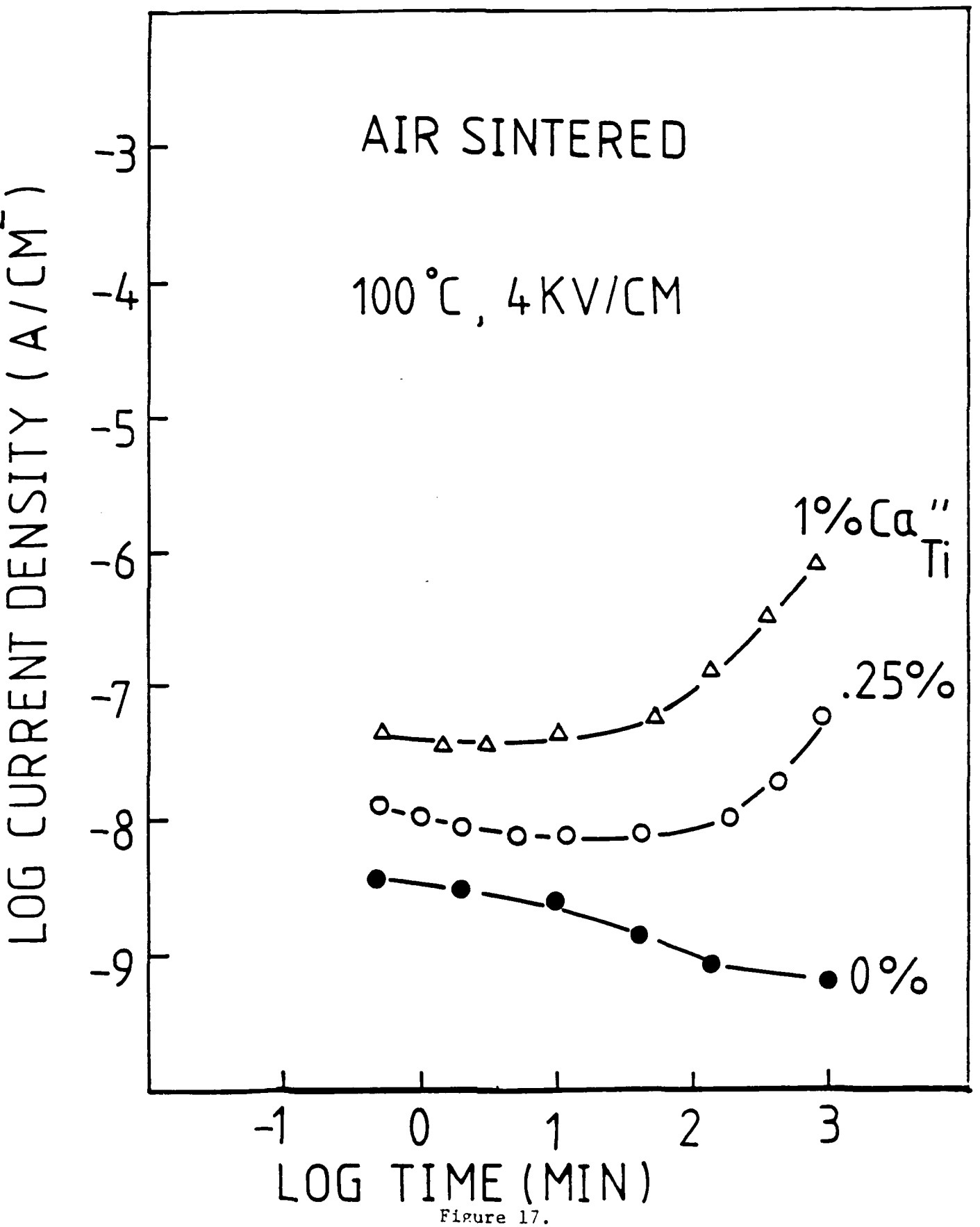
AIR SINTERED
100°C, 4KV/CM
1% Ca" Ti
.25%
0%
LOG CURRENT DENSITY (A/CM2)
-3
-4
-5
-6
-7
-8
-9
-1
0
1
2
3
LOG TIME (MIN)

Figure 17.

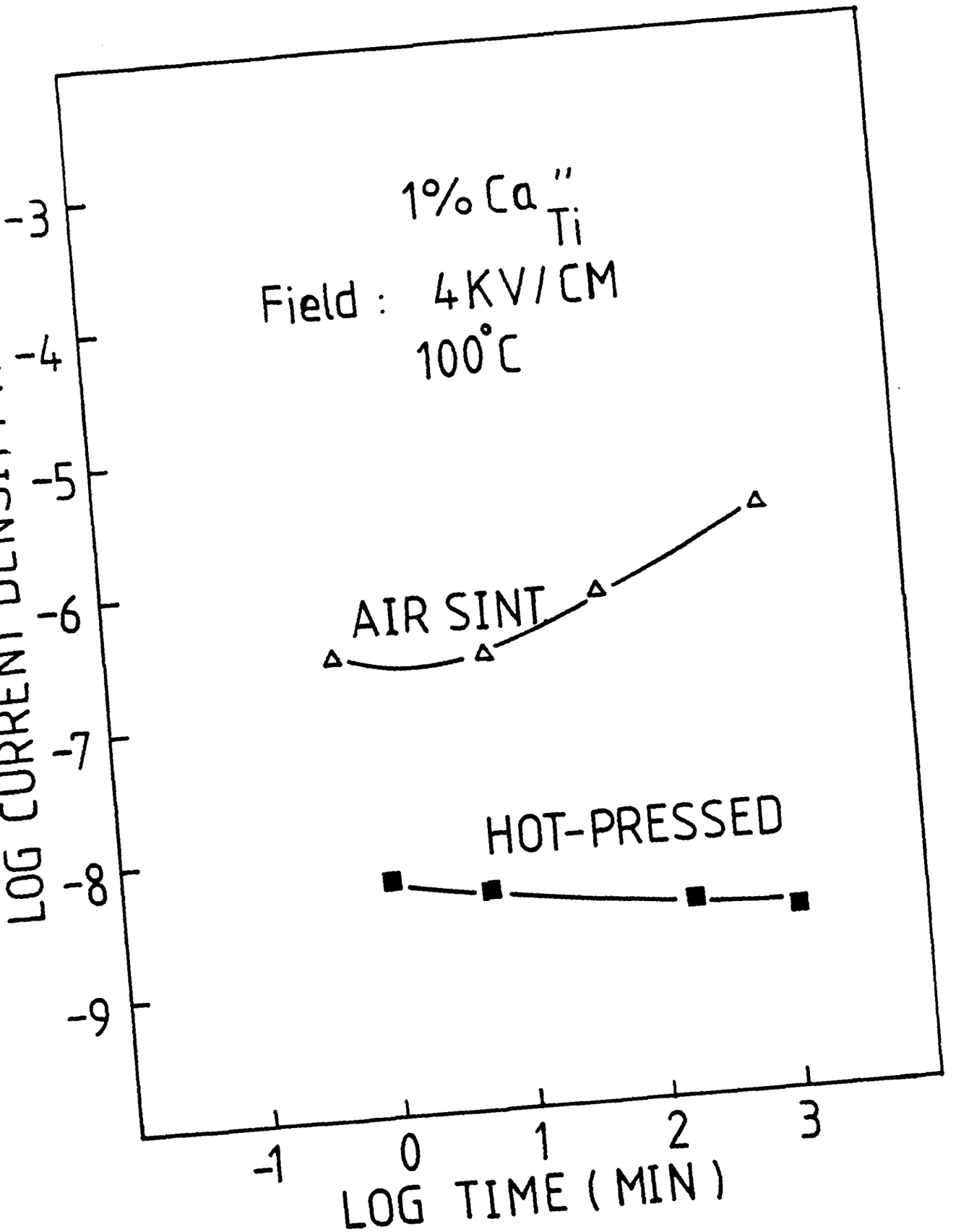
1% Ca
Ti
Field : 4KV/CM
100°C
AIR SINT
HOT-PRESSED
LOG CURRENT DENSITY (A/CM²)
-3
-4
-5
-6
-7
-8
-9
-1
0
1
2
3
LOG TIME (MIN)

Figure 18.

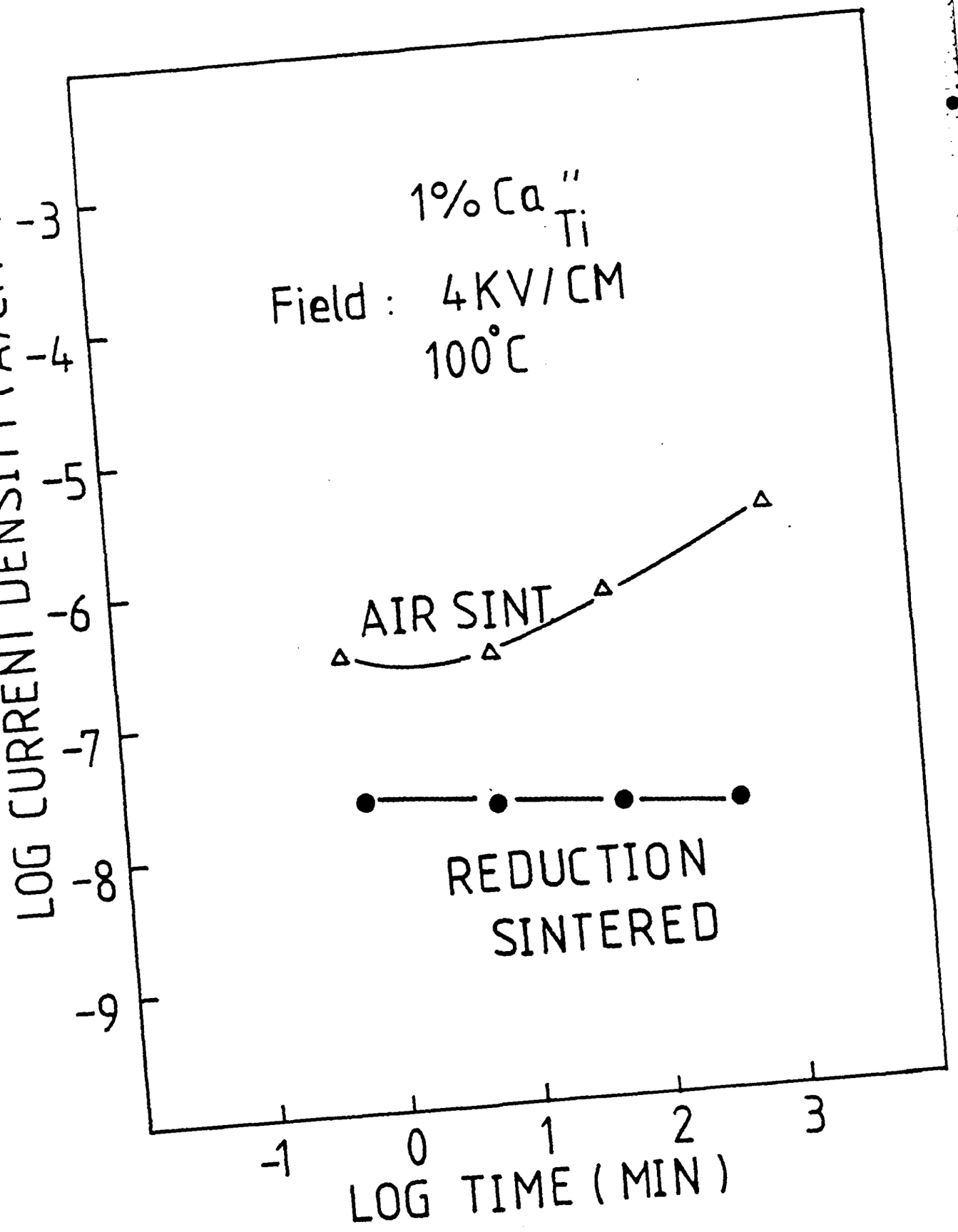
1% Ca
Ti
Field : 4KV/CM
100°C
AIR SINT
REDUCTION
SINTERED
LOG CURRENT DENSITY (A/CM 2)
-3
-4
-5
-6
-7
-8
-9
-1
0
1
2
3
LOG TIME (MIN)

Figure 19.

APPENDIX A

SOLUBILITY OF BaO in $BaTiO_3$

Y. H. Hu, M. P. Harmer, and D. M. Smyth

Materials Research Center, No. 32

Lehigh University

Bethlehem, PA 18015

To be presented at the Fall Meeting of the American Ceramic Society, Joint Electronics and Basic Science Division Meeting, San Francisco, October 28-31, 1984.

ABSTRACT

The solubility and mode of incorporation for BaO in $BaTiO_3$ has been studied by x-ray powder diffraction, scanning and transmission electron microscopy, electron probe microanalysis and equilibrium electrical conductivity. The presence of barium orthotitanate, Ba_2TiO_4, as a second phase for samples containing $\geq$0.1 mol percent excess BaO has been confirmed by direct microscopic examination. There was no evidence to support the incorporation of excess BaO in $BaTiO_3$ by a Ruddlesden-Popper type of superlattice ordering mechanism. Measurement of the equilibrium electrical conductivity showed no detectable shift in the conductivity profile due to BaO-excess, and this sets an upper limit of 100 ppm for the solubility of BaO in $BaTiO_3$.

1. Introduction

Until now, relatively little has been known about the solubility or mode of incorporation of excess BaO in $BaTiO_3$. A phase diagram for the system BaO-TiO_2 has been reported by Rase and Roy[1], however, they did not investigate any compositions between Ba/Ti ratios of 1.000 and 1.083. Accordingly, even though this phase diagram shows no solubility for BaO in $BaTiO_3$ over the temperature range 1200-1600°C, the precise solubility limit for BaO in $BaTiO_3$ and its mode of incorporation (random solid solution or ordered) has not previously been determined.

Possible point defect incorporation reactions for the accommodation of excess BaO into the $BaTiO_3$ lattice are as follows:

$$BaO \rightarrow Ba_{Ba}^{x} + V_{Ti}^{''''} + O_{o}^{x} + 2V_{o}^{\cdot\cdot} \qquad (1)$$

$$BaO \rightarrow Ba_{i}^{\cdot\cdot} + O_{i}^{''} \qquad (2)$$

$$2BaO \rightarrow Ba_{Ba}^{x} + Ba_{Ti}^{''} + 2O_{o}^{x} + V_{o}^{\cdot\cdot} \qquad (3)$$

The defect notation is that proposed by Kroger and Vink.[2] Equation (2) is an unlikely option since large interstitial ions are considered unfavorable in the close-packed perovskite structure. Equation (3) is unlikely because of the size mismatch between Ba^{++} and the titanium site, but it must be considered since it has been determined that Ca^{++} ions can be made to occupy titanium sites in $BaTiO_3$.[3]

An alternative mechanism for accommodating excess BaO in $BaTiO_3$ is by structural modification of the type described by Ruddlesden and Popper for the case of SrO-excess $SrTiO_3$.[4] In $SrTiO_3$, large excesses of SrO can be accommodated by insertion of individual layers of SrO between blocks of perovskite structure. These ordered structures correspond to a

homologous series of compounds, $SrO \cdot nSrTiO_3$, where n corresponds to the number of perovskite layers (TiO_6 octahedra) between SrO layers. Such structures have been directly observed in the transmission electron microscope by Tilley.[5]

The purpose of the present study has been to apply a wide range of analytical techniques including x-ray diffraction, scanning and transmission electron microscopy, electron probe microanalysis, and equilibrium electrical conductivity to clarify the solubility of, and mode of incorporation for, BaO in $BaTiO_3$.

2. Experimental Procedure

Starting powders were prepared by the liquid-mix technique, starting with titanium tetraisopropoxide and barium carbonate. This technique which allows precise and accurate control of the Ba/Ti ratio, is a modification of a process developed by Pechini,[6] and has been described elsewhere.[7,8] Compositions were prepared having Ba/Ti ratios varying from 1.000 to 1.100.

The ultra-fine powders were hot pressed into fully dense samples for the x-ray diffraction and microscopy work. Hot pressing was conducted inside a graphite resistance heated furnace using high purity graphite dies (99.99%), high purity alumina spacers and TZM superalloy punches. The inner die walls and contact surfaces of the spacers were coated with a thin layer of high purity boron nitride to prevent solid state reaction between the barium titanate, alumina and graphite. Approximately five grams of powder was used to press each disc. The hot pressing conditions (temperature, pressure, time to reach full density) were 1200°C, 45 MPa, 50 minutes for compositions having Ba/Ti ratios of 1.100 and 1.040, and

1200°C, 45 MPa, 30 minutes for compositions having Ba/Ti ratios of 1.000 and 1.002. The atmosphere in the hot press was flowing nitrogen gas. Coarsened grain structures were produced by subsequently annealing the hot pressed samples for 48 hours at 1100°C in air.

Pressureless sintered samples were prepared for the conductivity studies. Powders were cold pressed into rectangular bars and sintered in air at 1420°C for 2-1/2 hours. Polished sections for microscopic examination were prepared by diamond polishing in a medium of absolute ethanol. Water was determined to be an inappropriate polishing medium for BaO-excess $BaTiO_3$ since the second phase, Ba_2TiO_4, hydrolyzes rapidly in water and is leached out of the sample. (This explains why a second phase is usually not visible in published micrographs of BaO-rich $BaTiO_3$.[9]) Grain structures were revealed by thermal etching at 1050°C for one hour. Polished surfaces were examined by scanning electron microscopy (ETEC Autoscan) and by wavelength dispersive spectroscopy in an electron microprobe (JEOL 733 superprobe).

Thin foil specimens for transmission electron microscopy were prepared by ion-beam milling and examined in a Philips 400T electron microscope equipped with an energy dispersive x-ray analyzer.

The equilibrium electrical conductivities were measured by 4-point dc technique using platinum electrodes. A stabilized zirconia oxygen activity cell was used to measure the wide range of oxygen partial pressures obtained from $Ar-O_2$ and $CO-CO_2$ gas mixtures.

Ground samples were prepared for x-ray powder diffraction studies. Powders were examined using a Philips APD 3600 powder diffractometer operating at 45 kV, 30 mA and 0.01 degrees per second scan rate with CuK_α radiation.

3. Results

3.1 X-ray Diffraction

Specimens having Ba/Ti ratios of 1.000, 1.001, 1.002, 1.040 and 1.100 were examined by x-ray diffraction. A barium rich second phase, identified as barium orthotitanate, Ba_2TiO_4, was detected in compositions having Ba/Ti ratios of 1.100 and 1.040. X-ray diffractograms for samples with compositions Ba/Ti = 1.000 and 1.100 are shown in Figure 1 for comparison.

3.2 Scanning Electron Microscopy

Figures 2(A-E) show secondary electron images of microstructures for polished and thermally etched samples with Ba/Ti ratios, 1.000, 1.001, 1.002, 1.04 and 1.10. Second phase particles, mostly at the grain boundaries, are clearly visible for all samples with the exception of the stoichiometric composition (Ba/Ti = 1.000). The particles are easy to observe since they push up out of the grain boundaries during thermal etching and concentrate on the surface as discrete protruberances (compare figures 2 and 3).

Figures 3 (A-E) show backscattered scanning electron images for polished and unetched samples with Ba/Ti ratios, 1.000, 1.001, 1.002, 1.040 and 1.100. The second phase particles are noticeable in all of the nonstochiometric compositions due to the brighter contrast they produce in this mode of imaging. The high brightness of the second phase particles verifies that they are barium-rich since the backscattered electron intensity is higher for higher atomic number elements. Note that the presence of small barium rich particles can be detected even for samples containing an excess of only 0.1 mol % BaO.

3.3 Electron Probe Microanalysis

The composition of the barium rich second phase for samples with Ba/Ti ratios of 1.100 and 1.040 was studied by wavelength-dispersive electron microprobe analysis (EPMA). A typical line scan result for samples with Ba/Ti = 1.100, is shown in figure 4 which confirms a barium enrichment within the second phase particles.

The precise composition of the barium rich particles was determined using the standard ZAF correction technique.[10] Using the matrix phase ($BaTiO_3$) for calibration purposes, the composition of the barium-rich second phase was determined to be 71.8$\pm$ 1.32 % Ba and 12.37 $\pm$ 0.01 % Ti (by weight). This corresponds to the phase composition for barium orthotitanate (71.05 % Ba, 12.4 % Ti). Accordingly, the BaO-rich second phase was concluded to be barium orthotitanate, Ba_2TiO_4.

3.4 Transmission Electron Microscopy

Selected samples were examined by transmission electron microscopy. Figure 5 shows a bright field image for a sample with a Ba/Ti ratio of 1.100. Individual grains were analyzed using quantitative energy dispersive x-ray microanalysis (EDX) and this showed that some of the grains (marked B_2T on the micrograph) had compositions corresponding to barium orthotitanate. Selected area diffraction patterns from the orthotitanate grains showed an ordered structure within those grains (see figure 6). Lattice fringe imaging of the ordered structure within the Ba_2TiO_4 grains (figure 7) revealed a superlattice periodicity of 2·3 nm, three times the b-axis unit cell dimension for Ba_2TiO_4.

No ordering was observed within the $BaTiO_3$ matrix grains. Figures 8 (A and B) show selected area diffraction patterns taken from the $BaTiO_3$ matrix grains. From this it can be seen that none of the patterns show any extra reflections

of the superlattice type verifying that ordering was restricted to the Ba_2TiO_4 phase only.

3.5 Equilibrium Electrical Conductivity

Equilibrium electrical conductivity profiles measured at 1000°C for samples with Ba/Ti ratios, 1.000, 1.001, 1.002 and 1.005 are shown in figure 9. Note that there is no discernable shift in the conductivity profile that could be attributed to an increase in $[V_o^{\bullet\bullet}]$ due to solubility of excess BaO according to Equations (1) and (3).

4. Discussion

The observation of Ba_2TiO_4 in $BaTiO_3$ containing an excess of $\overline{>}0.1$ mol % BaO indicates that accommodation of excess BaO according to a Ruddlesden-Popper type of superlattice does not occur in $BaTiO_3$. This was further substantiated by the results of the TEM selected area diffraction analysis that revealed no signs of superlattice ordering within the $BaTiO_3$ grains in BaO-excess $BaTiO_3$. The microscopy results also confirmed that the solubility of BaO must be less than 0.1 mol % since a second phase was observable for samples having $\geq$ 0.1 mol% excess BaO, (Ba/Ti $\geq$ 1.001).

More precise information on the solubility limit can be deduced from the electrical conductivity data. Measurement of the equilibrium electrical conductivity is a sensitive test for changes in the concentration of extrinsic oxygen vacancies as would occur by incorporation of excess BaO according to equations (1)-(3). Changes in $[V_o^{\bullet\bullet}]$ of the order of 100 ppm can be detected.[11] As shown in figure 10, there is no shift in the conductivity profile in the presence of excess BaO. In conclusion, the solubility of excess BaO in $BaTiO_3$ is < 100 ppm, and is insufficient to modify the defect concentrations relative to the natural impurity content Finally, since $V_o^{\bullet\bullet}$ is known to be easily formed in $BaTiO_3$, it can be deduced from

equations (1), (2) and (3) that $V_{Ti}^{''''}$, $Ba_i^{\circ\circ}$, $O_i^{\circ\circ}$ and $Ba_{Ti}^{''}$ are, by comparison to $V_O^{\circ\circ}$, energetically unfavorable defects in $BaTiO_3$. As mentioned earlier we would expect interstitial defects to be unfavorable due to the close packed nature of the perovskite structure. Similarly, incorporation of large Ba^{++} ions on Ti-sites as $Ba_{Ti}^{''}$ would be difficult. Cation vacancies have long been recognized as unfavorable defects in $BaTiO_3$, although recent work has shown that $V_{Ti}^{''''}$ is more favorable than $2V_{Ba}^{''}$ and that $V_{Ti}^{''''}$ is in fact the preferred compensating defect for highly donor doped $BaTiO_3$.[12,13] Nevertheless, the measured low solubility of BaO in $BaTiO_3$ is in accord with the fact that all of the options for the incorporation of excess BaO by point defect formation involve energetically unattractive defect types.

5. Conclusions

The solubility of BaO in $BaTiO_3$ has been determined to be no more than 100 ppm. A second phase comprising barium orthotitanate Ba_2TiO_4 was observed for all samples having Ba/Ti ratios $\geq$1.001. Incorporation of excess BaO by a Ruddlesden-Popper type of superlattice does not occur in $BaTiO_3$.

Acknowledgement

This research was supported by the Ceramics Program, Division of Materials Research, Office of Naval Research. The authors appreciate the assistance of Dr. Helen Chan with the transmission electron microscopy.

References

1. D. E. Rase and R. Roy, "Phase Equilibria in the System BaO-TiO_2," J. Am. Ceram. Soc., 38 [3], 102-13 (1955).
2. F. A. Kroger and H. J. Vink, p. 307 in Solid State Physics, Vol. 3, Edited by F. Seitz and D. Turnbull, Academic Press, New York (1956).
3. H. Chan, M. P. Harmer, M. Lal and D. M. Smyth, "Calcium Site Occupancy in $BaTiO_3$," Mat. Res. Soc. Symp. Vol. 31 (1984).
4. S. N. Ruddlesden and P. Popper, Acta Crystallogr., 11, 54 (1958).
5. R. J. D. Tilley, J. Solid State Chem., 21, 293 (1977).
6. M. Pechini, U.S. pat. 3,330,697 (1967).
7. R. K. Sharma, N. H. Chan and D. M. Smyth, J. Am. Ceram. Soc., 64, 448 (1981).
8. N. H. Chan, R. K. Sharma and D. M. Smyth, J. Electrochem. Soc., 128, 1762 (1981).
9. R. K. Sharma, N. H. Chan and D. M. Smyth, "Solubility of TiO_2 in $BaTiO_3$," J. Am. Ceram. Soc., 64[8], 448 (1981).
10. J. I. Goldstein, et al. Scanning Electron Microscopy and X-ray Microanalysis, Chapter 7, Plenum Press, New York (1981).
11. N. H. Chan, R. K. Sharma and D. M. Smyth, "Nonstoichiometry in Acceptor-Doped $BaTiO_3$," J. Am. Ceram. Soc., 65 [3], 167-70 (1982).
12. H. Chan, M. P. Harmer and D. M. Smyth, "Electron Microscopy of Nb-doped $BaTiO_3$," to be submitted to J. Am. Ceram. Soc.: for Abstract see Am. Ceram. Soc. Bull., 63 [3], 482 (1984)
13. G. H. Jonker and E. E. Havinga, "The Influence of Foreign Ions on the Crystal Lattice of Barium Titanate," Mat. Res. Bull., vol. 17, 345-50 (1982).

Figure Captions

Figure 1: Partial x-ray diffractograms for samples having Ba/Ti ratios of 1.000 (A) and 1.100 (B). The extra (022) and (200) reflections for the excess BaO sample are due to Ba_2TiO_4.

Figure 2: Scanning electron micrographs (secondary electron imaging mode) for polished and thermally etched samples having Ba/Ti ratios of 1.000 (A), 1.001 (B), 1.002 (C), 1.04 (D) and 1.10 (E). Note the presence of protruding precipitates in all of the nonstoichiometric compositions.

Figure 3: Scanning electron micrographs (backscattered electron imaging mode) for polished only samples having Ba/Ti ratios of 1.000 (A), 1.001 (B), 1.002 (C), 1.04 (D) and 1.10 (E). The barium rich particles show up with bright contrast in all of the nonstoichiometric compositions.

Figure 4: Microprobe x-ray line scan for sample having Ba/Ti = 1.100 verifying barium enrichment within solid second phase particles.

Figure 5: Bright field transmission electron micrograph of a sample having Ba/Ti = 1.100. The grains marked B_2T were identified as barium orthotitanate, Ba_2TiO_4.

Figure 6: Selected area diffraction pattern taken from a barium orthotitanate grain shown in figure 6. Note the presence of extra superlattice reflections.

Figure 7: Lattice fringe image showing on ordered structure with a 2·3 nm periodicity within a Ba_2TiO_4 grain in a sample having a Ba/Ti ratio of 1.100.

Figure 8: Selected area diffractionpatterns for [001] and [111] zone axis orientations taken from $BaTiO_3$ matrix grains for samples having a Ba/Ti ratio 1.100. Note the absence of extra reflections of the superlattice type.

Figure 9: Equilibrium electrical conductivity at 1000°C for stoichiometric and BaO-excess $BaTiO_3$.

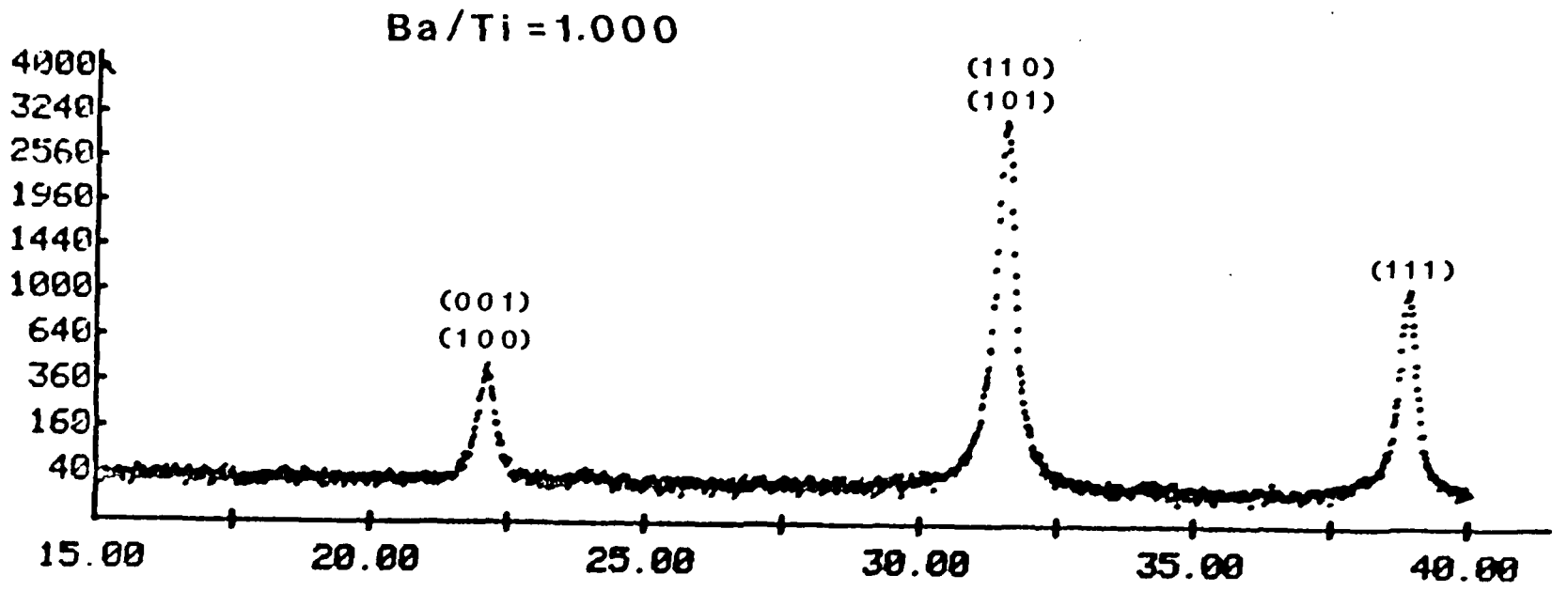
Ba/Ti =1.000
4000
3240
2560
1960
1440
1000
640
360
160
40
(001)
(100)
(110)
(101)
(111)
15.00
20.00
25.00
30.00
35.00
40.00

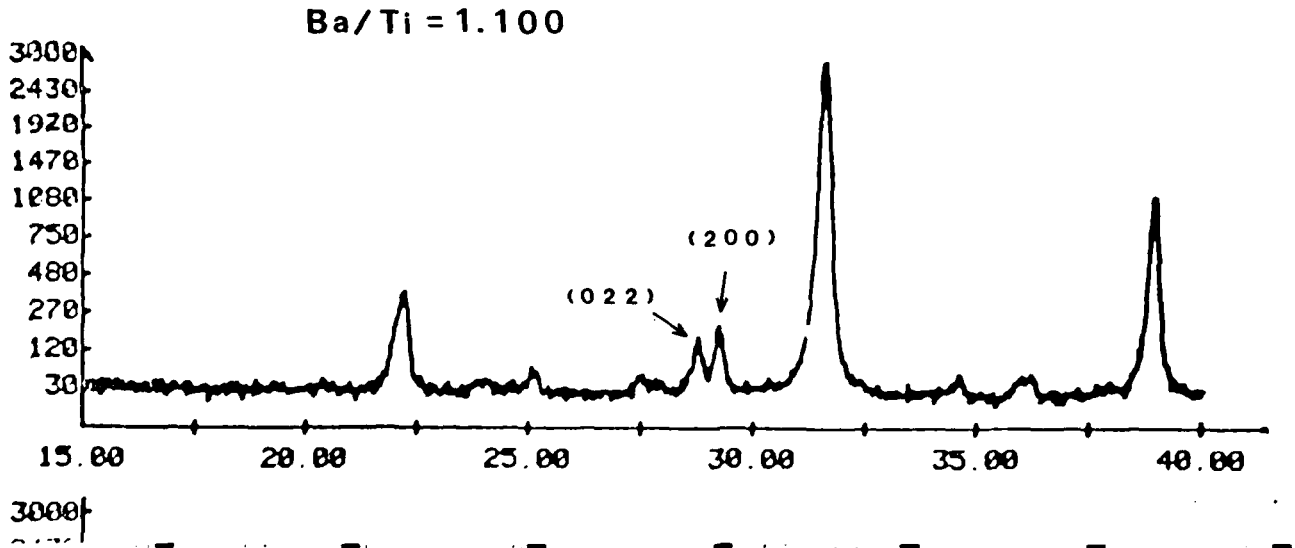
Ba/Ti = 1.100
3000
2430
1920
1470
1080
750
480
270
120
30
(022)
(200)
15.00
20.00
25.00
30.00
35.00
40.00
3000

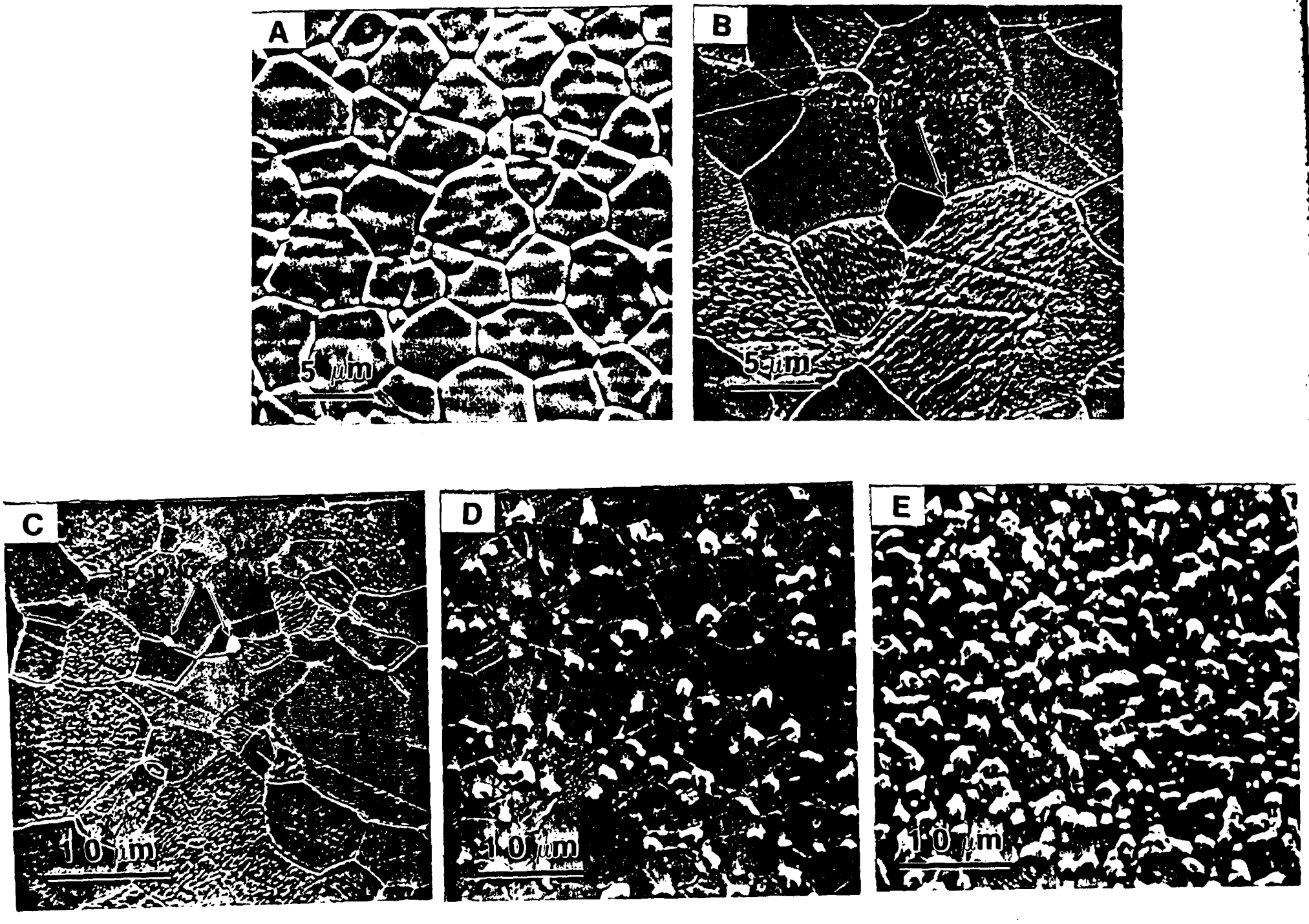
A
5 μm
B
5 μm
C
10 μm
D
10 μm
E
10 μm

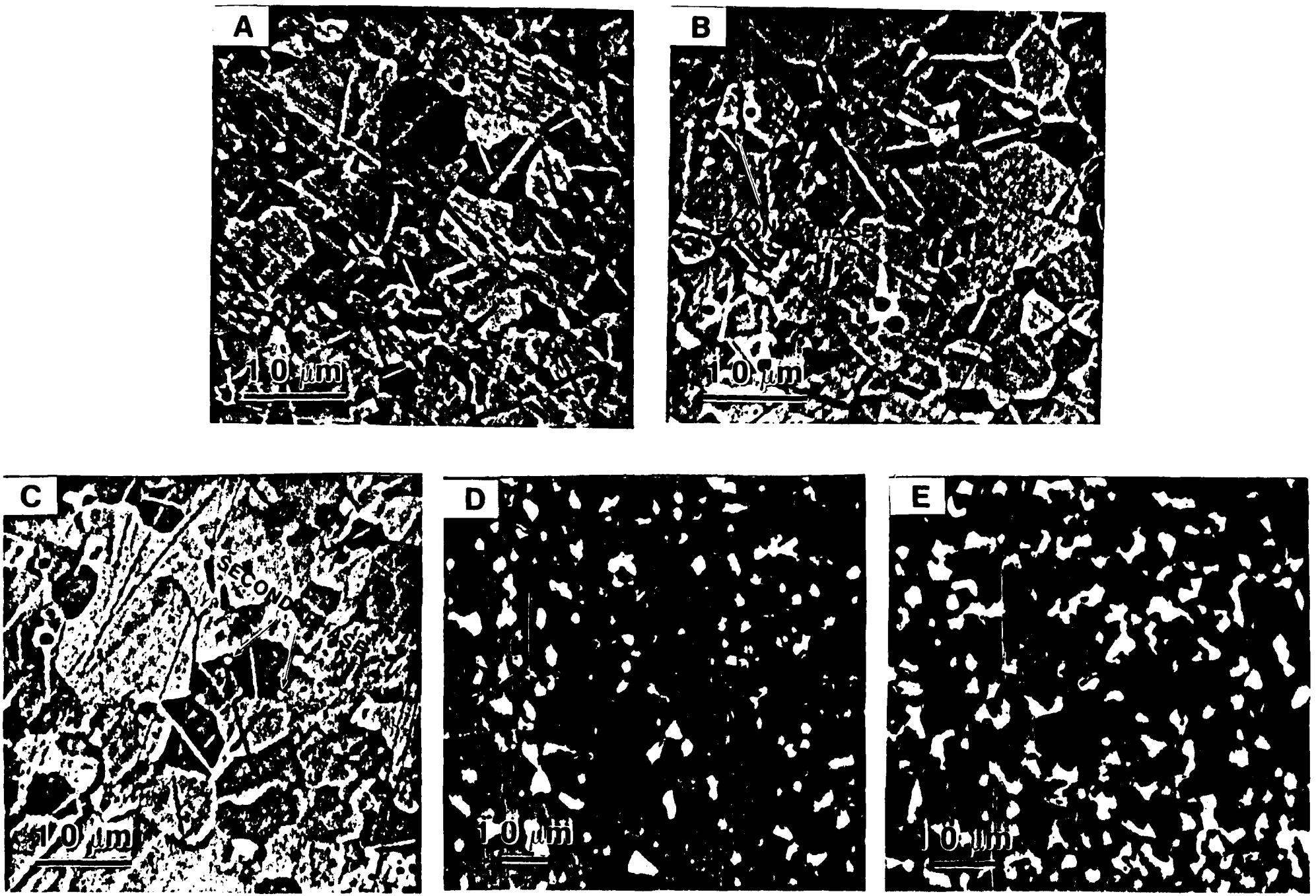
A
10 μm
B
10 μm
C
SECOND PHASE
10 μm
D
10 μm
E
10 μm

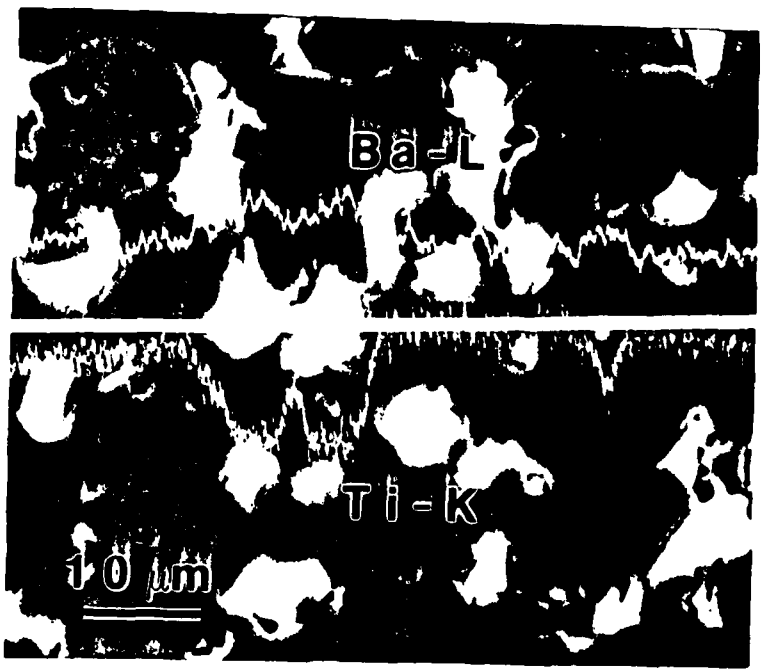
Ba-L
Ti-K
10 μm


B2T
B2T
B2T
B2T
B2T
1.0 μm

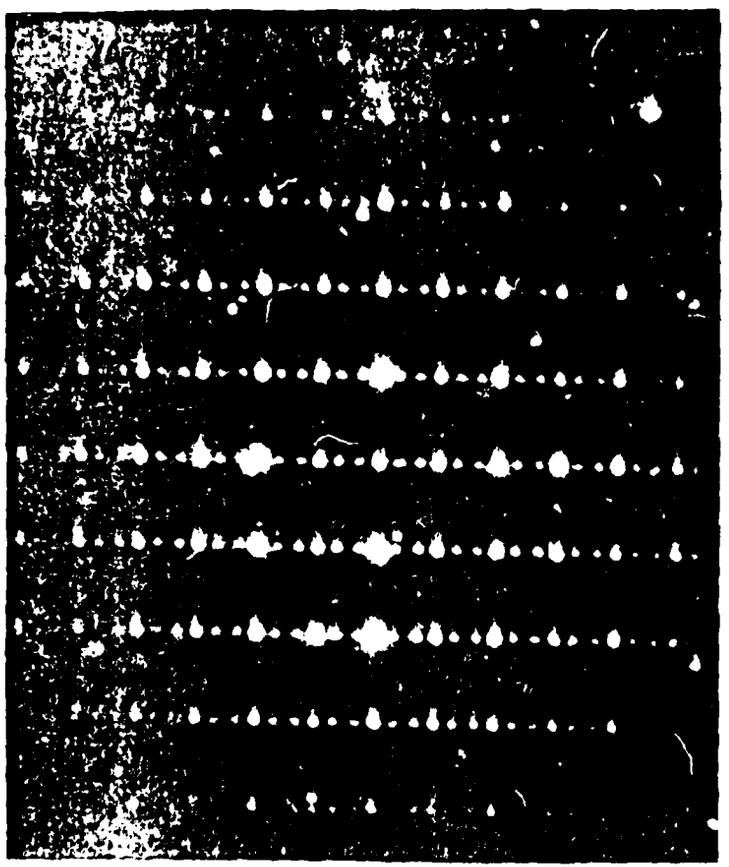

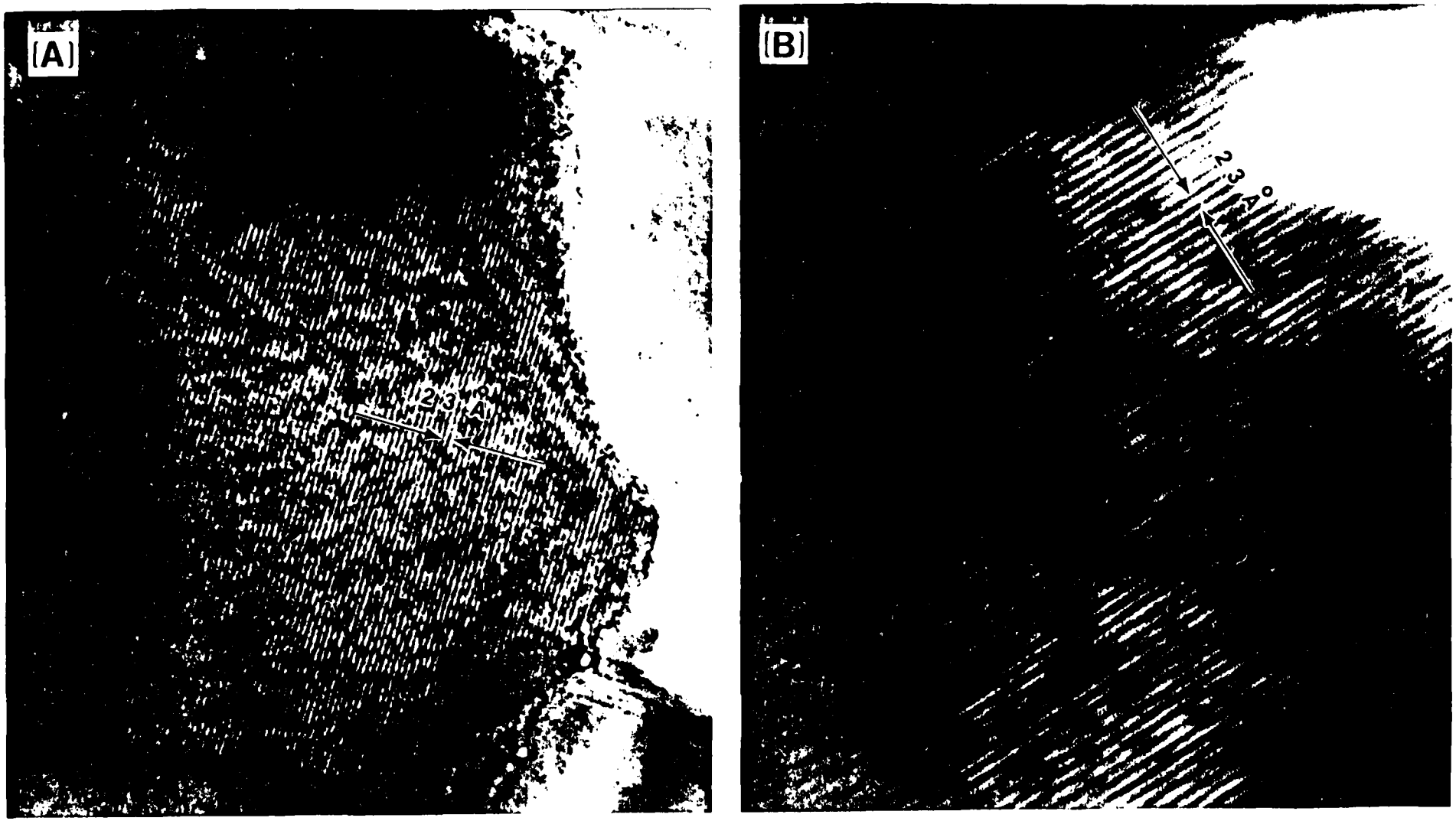
(A)
2.3 A°
(B)
2.3 A°

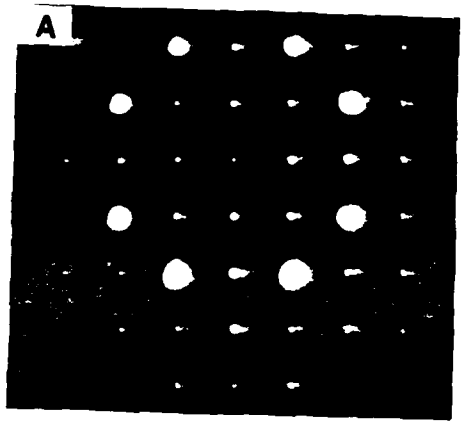
A

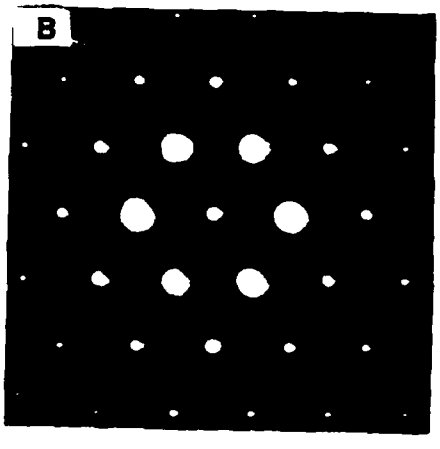
B

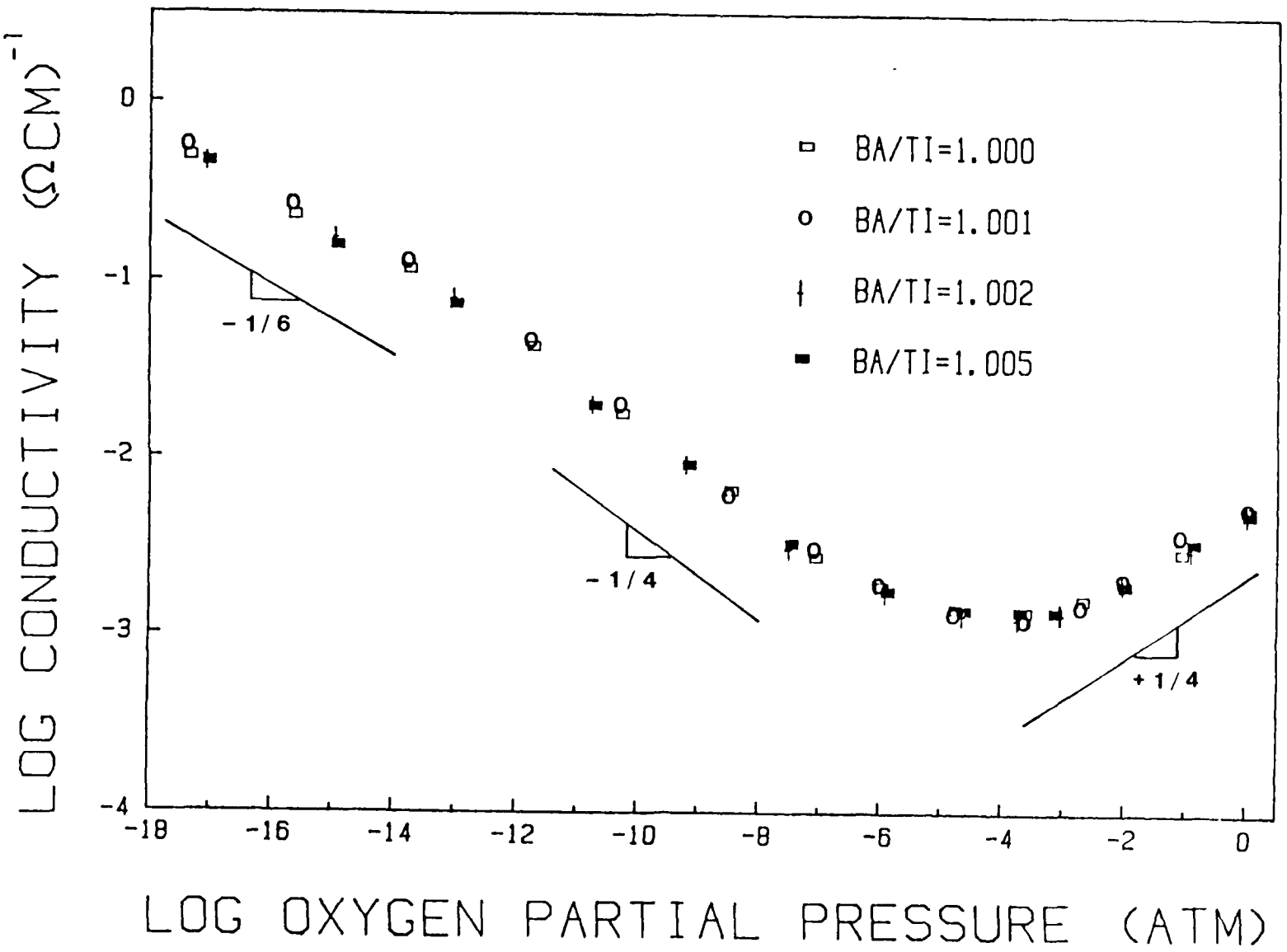
LOG CONDUCTIVITY (ΩCM)$^{-1}$
0
-1
-2
-3
-4
-18
-16
-14
-12
-10
-8
-6
-4
-2
0
BA/TI=1.000
BA/TI=1.001
BA/TI=1.002
BA/TI=1.005
-1/6
-1/4
+1/4
LOG OXYGEN PARTIAL PRESSURE (ATM)

AEM Determination of the Compensating Defect Mechanism in Highly Donor Doped $BaTiO_3$

Helen M. Chan, M. P. Harmer and D. M. Smyth

Introduction

It is well known that when $BaTiO_3$ is donor-doped, there is a transition from semi-conducting to insulating behaviour as the concentration of donor is increased [1]. For Nb as the donor dopant, the transition occurs at ~ 0.5 mol%Nb. For compositions $BaTi_{(1-x)}Nb_xO_3$ ($x < 0.5$ mol%), the semi-conducting behaviour can be accounted for by the following defect eqn. -

$$2\ BaO + Nb_2O_5 \rightarrow 2\ Ba_{Ba}^{X} + 2\ Nb_{Ti}^{\bullet} + 6O_o^{X} + 1/2\ O_2(g) + 2e^{-} \qquad \text{Eqn. 1}$$

The niobium ions occupy Ti sites, and because of its higher valency, a niobium ion on a Ti site can be considered to possess a single positive charge. For every two niobium atoms, there is one oxygen atom which is excess in the perovskite lattice. For the low Nb concentrations, this oxygen is given off, leaving behind two electrons, hence the semi-conducting behaviour.

As the Nb concentration is increased however, the material becomes insulating. This implies therefore that the oxygen which was given off previously, is now being retained within the lattice, and this has been confirmed by gravimetric measurements [1]. Various models can be put forward to account for how the extra oxygen is accommodated in the lattice. These will be discussed in turn:

1. Ba vacancy model

$$Nb_2O_5 + 2\ BaO \rightarrow 2\ Nb_{Ti}^{\cdot} + 6O_O^X + Ba_{Ba}^X + V_{Ba}^{''} + BaO \qquad \text{Eqn. 2}$$

In this model the niobium is compensated by the creation of a Ba vacancy. The "freed" Ba ion then combines with the extra oxygen to form a barium rich second phase. This second phase could take various forms, it might occur discretely e.g., $BaO + BaTiO_3 \rightarrow Ba_2TiO_4$, or it could exist as a Ruddlesden-Popper type phase [2,3] where the BaO occurs as planes between the perovskite layers.

2. Direct incorporation of the oxygen ion into the lattice.

3. Titanium vacancy model.

$$4\ BaO + 2\ Nb_2O_5 + 2\ BaTiO_3 \rightarrow 4\ Nb_{Ti}^{\cdot} + 6\ Ba_{Ba}^X + Ti_{Ti}^X + V_{Ti}^{''''} + 18O_O^X + TiO_2 \qquad \text{Eqn. 3}$$

This is equivalent to the Ba vacancy model except that in this case, compensation of the niobium is achieved by the creation of a titanium vacancy, and hence a titanium rich second phase is formed.

The purpose of this study therefore was to examine the structure of Nb doped $BaTiO_3$ in the AEM/TEM, and by careful control of the compositions studied, determine which of the above models is correct.

Experimental Procedure

The compositions studied are shown in Table 1. The reasoning behind the choice of the non-stoichiometric compositions will be made clear in the discussion section. The specimens were made up using a liquid mix technique which has been described fully elsewhere [4]. The pressed pellets were sintered in air at 1450°C for 5 hours, and then furnace cooled. TEM

specimens were prepared by ion-beam milling, and examined in a Philips 400T electron microscope equipped with an energy dispersive X-ray analyser.

Results

The results from the stoichiometric compositions (Ba/(Ti + Nb) = 1) will be considered first.

0.25 mol% Nb

The structure of the 0.25 mol% Nb specimen was single-phase, and contained a large number of ferroelectric domains (see Fig. 1). Of the compositions studied, this is the only specimen which showed ferroelectric domain contrast. This is because the higher Nb concentrations suppress the ferroelectric transition so that the high temperature cubic structure is retained.

6, 8 mol% Nb

The 6 and 8 mol% Nb specimens had similar structures (see Fig. 2). Ordering within the grains was checked for by looking for superlattice reflections in the diffraction pattern, however none were detected. An intergranular second phase was observed. This was readily distinguished either by its morphology, or by its diffraction pattern--the lattice spacing of the second phase was significantly larger than that of the matrix. Using X-ray EDS it was found that the second phase was titanium rich, the ratio of Ti to Ba being ~ 2.3. The second phase was also found to contain Nb. The concentration of Nb was 1-1.5X the dopant concentration in the matrix.

Nonstoichiometric

a) Barium Deficient $Ba_{.97}Ti_{.94}Nb_{.06}O_3$

In this specimen there was a significant volume fraction of titanium rich second phase--see Fig. 3. X-ray analysis of these regions showed that

their composition was very similar to the Ti-rich second phase detected previously in the stoichiometric specimens.

b) Titanium deficient $BaTi_{.925}Nb_{.06}O_3$

The structure of the Ti deficient composition was completely free of any second phase, see Fig. 4.

Discussion

Stoichiometric compositions

The results from examining the 6 and 8 mol% Nb doped samples revealed the formation of a Ti rich second phase, thus indicating the Ti vacancy model to be more likely.

Non-stoichiometric compositions

a) $Ba_{.97}Ti_{.94}Nb_{.06}O_3$

This barium deficient composition was deliberately chosen so that in theory, exact compensation of the niobium could be achieved by existing barium vacancies in accord with the following defect equation:

$$BaO + Nb_2O_5 \rightarrow 2\ Nb_{Ti}^{\bullet} + Ba_{Ba}^{X} + V_{Ba}^{''} + 6O_O^X \qquad \text{Eqn. 4}$$

The results showed however that there was a significant quantity of second phase present, and that it was Ti rich. Thus even when the composition is barium deficient, compensation for the niobium is achieved by the creation of titanium vacancies. This can be represented as follows:

$$2BaO + 2Nb_2O_5 + 3\ BaTiO_3 \rightarrow 4\ Nb_{Ti}^{\bullet} + V_{Ti}^{''''} + 5\ Ba_{Ba}^{X} + 15O_O^X + 3\ TiO_2 \qquad \text{Eqn. 5}$$

In this case, there is the formation of a titanium rich second phase, which is what was observed experimentally.

b) $BaTi_{.925}Nb_{.06}O_3$

This composition is titanium deficient, and was chosen so that the niobium could be exactly compensated by titanium vacancies, without requiring

the formation of a second phase. Thus we have:

$$5BaO + 2\ Nb_2O_5 \rightarrow 4\ Nb_{Ti}^{\cdot} + V_{Ti}^{''''} + 5\ Ba_{Ba}^{X} + 15O_O^X \qquad \text{Eqn.6}$$

The experimental observations were in complete agreement with this.

General.

The results from all the compositions studied are consistent, and they provide strong evidence that the compensating defect in donor doped $BaTiO_3$ is the titanium vacancy $V_{Ti}^{''''}$, and not the barium vacancy. This result confirms the theoretical predictions of Catlow, who found that the energy of formation of a titamium vacancy was less than that of two barium vacancies [5]. Our results are also in agreement with the observations of Jonker et al. [6], who by accurately determining the composition of various single phase BaO-TiO_2-Nb_2O_5 mixtures, concluded that at 1200°C, the major compensation mechanism was the formation of Ti vacancies.

References

1. N. G. Eror and D. M. Smyth, "Oxygen Stoichiometry of Donor-Doped $BaTiO_3$ and TiO_2," pp. 62-74 in The Chemistry of Extended Defects in Non-Metallic Solids, L. Eyring and M. O'Keefe, Editors, North Holland, Amsterdam (1970).

2. S. N. Ruddlesden and P. Popper, Acta Crystallogr., 11, 54 (1958).

3. R. J. D. Tilley, J. Solid State Chem., 21, 293 (1977).

4. R. K. Sharma, N. H. Chan and D. M. Smyth, "Solubility of TiO_2 in $BaTiO_3$," J. Am. Ceram. Soc., 64[8], 448-51 (1981).

5. G. V. Lewis and C. R. A. Catlow, "Computer Modelling of Barium Titanate," Radiation Effects, 73, 307-14 (1983).

6. G. H. Jonker and E. E. Havinga, "The Influence of Foreign Ions on the Crystal Lattice of Barium Titanate," Mat. Res. Bull, 17, 345-350 (1982).

TABLE I

Composition	Description
$Ba\ Ti_{.9975}Nb_{.0025}O_3$	Stoichiometric .25 mol% Nb
$Ba\ Ti_{.94}Nb_{.06}O_{3.03}$	" 6 mol% Nb
$Ba\ Ti_{.92}Nb_{.08}O_{3.04}$	" 8 mol% Nb
$Ba_{.97}Ti_{.94}Nb_{.06}O_3$	Non-stoichiometric, barium deficient
$Ba\ Ti_{.925}Nb_{.06}O_3$	Non-stoichiometric, titanium deficient

Fig. 1. .25 mol % Nb.

Fig. 2. $BaTi_{.92}Nb_{.08}O_{3.04}$

Fig. 3. $BO_{.97}Ti_{.94}Nb_{.06}O_3$

Fig. 4. $BaTi_{.925}Nb_{.06}O_3$

a)

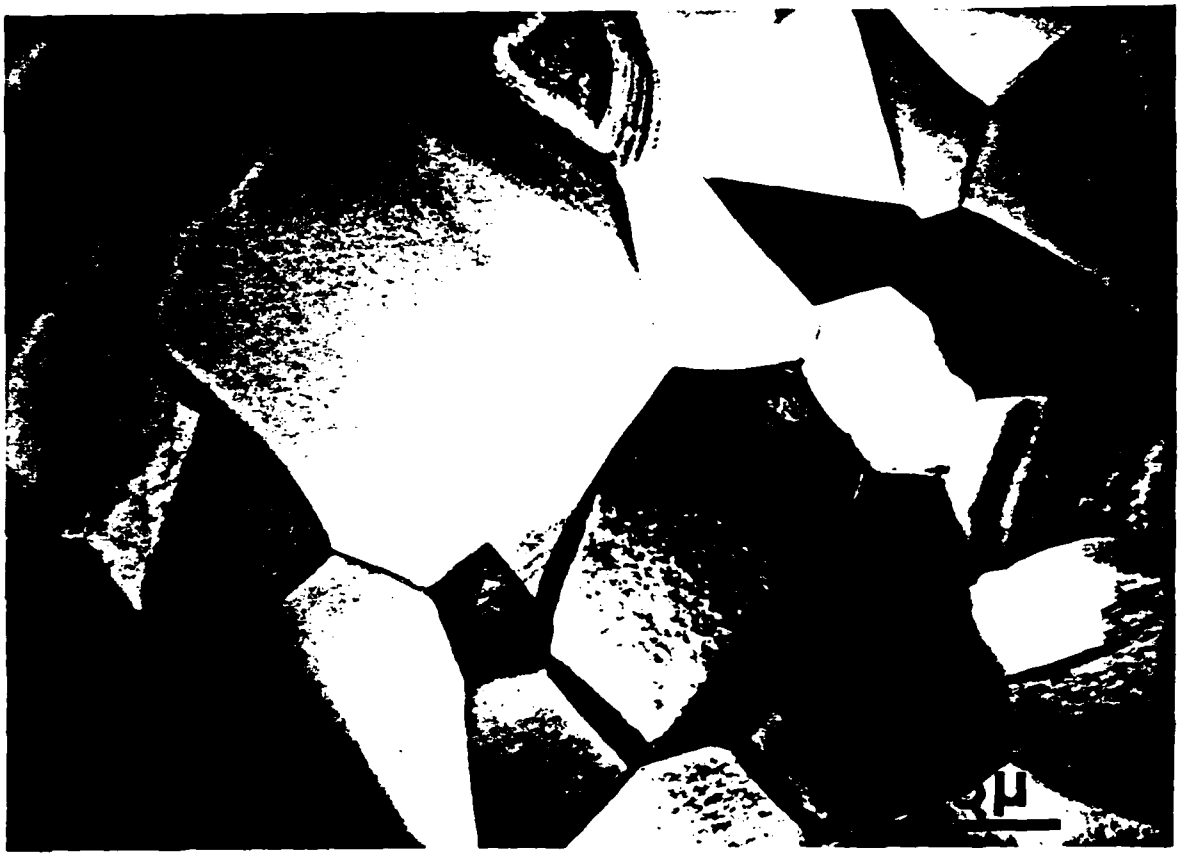

b)

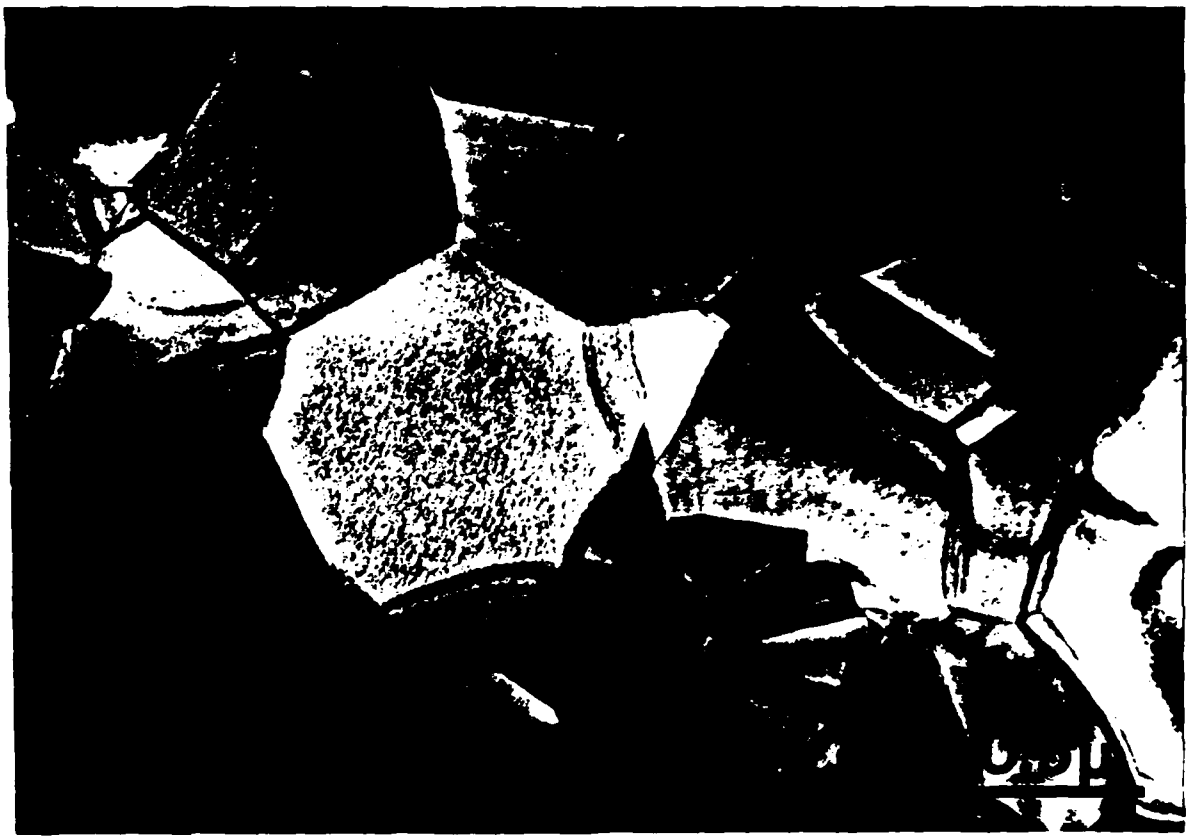

APPENDIX C

CALCIUM SITE OCCUPANCY IN $BaTiO_3$

H. M. Chan, M. P. Harmer, M. Lal, and D. M. Smyth
Materials Research Center, Lehigh University, Bethlehem, PA 18015 U.S.A.

ABSTRACT

Measurements of the equilibrium electrical conductivity of Ca-doped $BaTiO_3$ indicate a highly acceptor-doped behavior when $y > 1$ in the general formula $(Ba_{1-x}Ca_xO)_yTiO_2$. It has been suggested that when there is an excess of alkaline earth oxides, some Ca^{++} occupies Ti-sites, where it acts as a doubly charged acceptor, Ca_{Ti}''. This possibility has been checked with a recently developed technique for determining the crystallographic site occupancy of impurity atoms. Known as ALCHEMI (Atom Location Using Channeling-Enhanced Microanalysis), the technique relies on the dependence of the characteristic X-ray emission on the incident electron beam direction. A significant channeling effect was observed for slightly positive and negative excitations of the [100] reflection. The results indicate that for the composition $(Ba_{0.85}Ca_{0.15}O)_{1.02}TiO_{2.00}$, a substantial fraction of the total calcium ($\geq$ 20%) occupies Ti sites.

INTRODUCTION

A technique capable of determining the crystallographic site occupancy of impurity atoms has been recently developed [1]. The technique, known as ALCHEMI (Atom Location Using Channeling-Enhanced Microanalysis), relies on the dependence of the characteristic X-ray emission on the incident electron beam direction. ALCHEMI is well-suited to investigating the site occupancy of impurity atoms in $BaTiO_3$, because in this material, the barium and titanium atoms lie on alternate, parallel planes (<h00>). Thus depending on the incident beam orientation, the electron intensity will be concentrated at either the A or B planes, hence X-ray emission from one element will be enhanced relative to the other. By comparing the ratio of the characteristic X-ray intensity of an impurity element to that of either Ba or Ti for the two different orientations, it is possible to determine the fraction of impurity atoms on each type of site.

The interest in calcium-doped $BaTiO_3$ stems from its widespread use as a ceramic capacitor. Many commercial $BaTiO_3$ based multilayer capacitors contain significant amounts of calcium added by way of curie point shifters such as $CaZrO_3$. It has generally been assumed that when calcium is added to $BaTiO_3$, it substitutes for barium. However, during the course of a recent study of the high temperature (1000°C) equilibrium electrical conductivity of calcium-doped $BaTiO_3$, it was found that for A site excess compositions ((Ca + Ba)/Ti >1), calcium doping promoted acceptor type behavior [2]. Acceptor doping in $BaTiO_3$ leads to the formation of oxygen vacancies ($V_O^{\bullet\bullet}$) and a characteristic shift in the position of the minima on a plot of log conductivity vs. log $P_{O_2}(g)$ (see Fig. 1). The implication, therefore, is that for calcium-doped $BaTiO_3$, acceptor type behavior is caused by the presence of calcium on titanium sites (Ca_{Ti}'') and the resulting oxygen vacancy formation. Further support for the proposed mechanism comes from electrical degradation measurements [3]. It has been shown that calcium excess samples degrade more rapidly than their stoichiometric counterparts under conditions where degradation is believed to be controlled by $V_O^{\bullet\bullet}$ migration.

Mat. Res. Soc. Symp. Proc. Vol. 31 (1984)

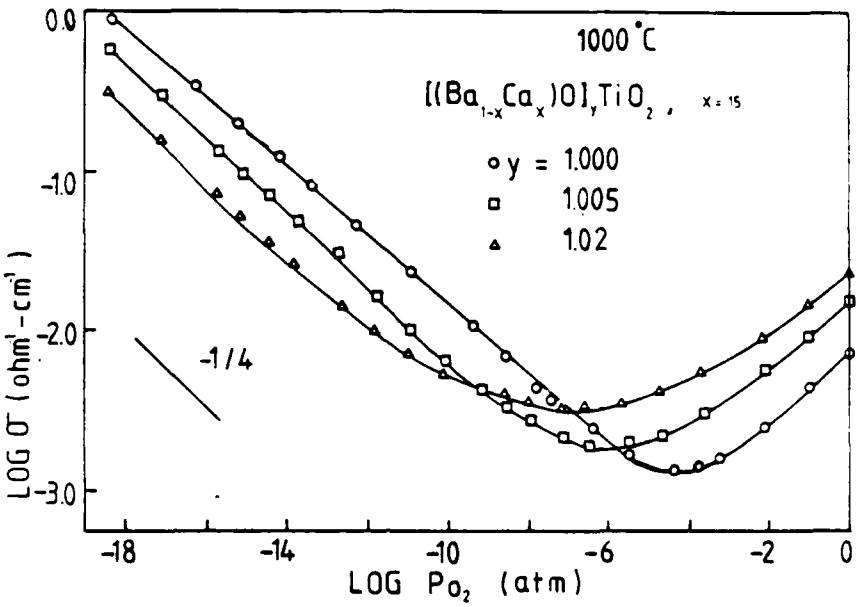

FIG. 1. Equilibrium electrical conductivity of Ca-doped $BaTiO_3$ at 1000°C.

All of the above measurements provide indirect evidence for the occupation of Ti atom sites by Ca atoms in $BaTiO_3$. Accordingly, the purpose of the present work has been to exploit the technique of ALCHEMI to obtain direct evidence and further quantitative information concerning the site occupancy for calcium ions in $BaTiO_3$.

EXPERIMENTAL PROCEDURE

Powders of precisely determined chemical composition were made by the liquid mix process which is described elsewhere [4]. Samples for electrical conductivity measurements were prepared by die pressing the powder into rectangular bars at 350 MPa followed by sintering in air at 1420°C for 2½ hours. All samples sintered well into the range of impermeability (≳ 95% theoretical density). The equilibrium electrical conductivity was measured using a four point d.c. technique which is described in detail elsewhere [4].

Thin foil specimens were prepare by ion beam milling, and examined in a Philips 400T electron microscope equipped with an EDAX energy dispersive X-ray analyzer. The specimen was tilted so that a systematic row of <h00> reflections was visible in the diffraction pattern. It was found that the most pronounced channeling effect occurred for slightly positive and slightly negative excitations of the [100] reflection (see Figs. 2a and b, respectively). These two orientations were used for collecting the X-ray spectra. It is worth noting, however, that in the ALCHEMI technique, the precise orientations within the systematic row are unimportant, providing sufficient channeling is obtained. The following two compositions were studied $(Ba_{1-x}Ca_xO)_yTiO_2$: y = 1.02 and 0.98; x = 0.15.

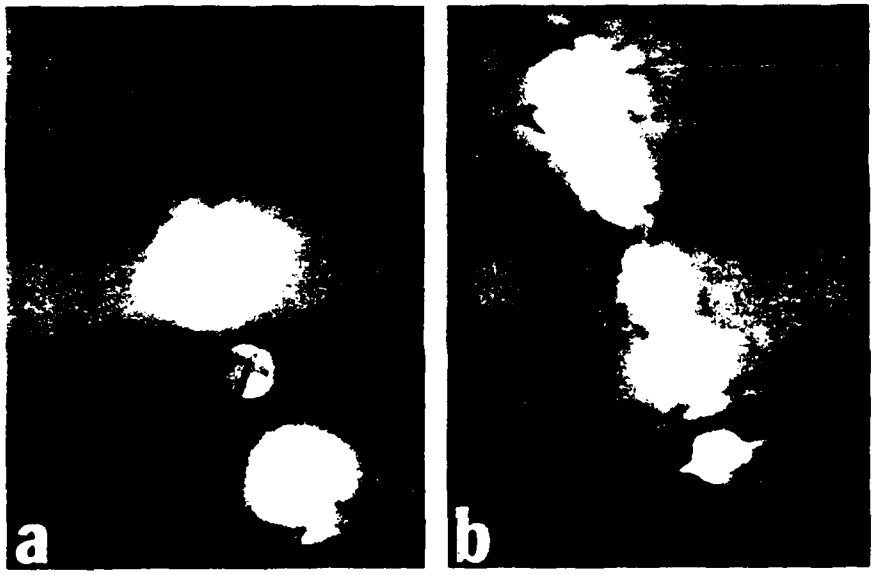

FIG. 2. Orientations used for ALCHEMI determination. a) S+, b) S-.

RESULTS

The microstructure of both specimens was similar, and consisted of fine grains ~5-10 μm in diameter. A large number of ferroelectric domains could also be observed (see Fig. 3).

The results of the ALCHEMI determination are shown in Table 1. C_x represents the fraction of Ca atoms occupying Ti sites, and was calculated from the following expression [1]:

$$C_x = (R-1)/(R-1+\gamma-\beta R)$$

where

$$R = (N_{Ba}^{(1)}/N_{Ca}^{(1)})/(N_{Ba}^{(2)}/N_{Ca}^{(2)}) \qquad (1)$$

$$\beta = N_{Ti}^{(1)}/kN_{Ba}^{(1)}$$

$$\gamma = N_{Ti}^{(2)}/kN_{Ba}^{(2)}$$

$k = N_{Ti}/N_{Ba}$ For an orientation in which there is no channeling.

The superscripts (1) and (2) represent the two orientations, and N is the number of counts in the X-ray peak.

It can be seen that the spread in C_x values was quite high, the reasons for this are discussed later. By applying a Student's t-test to the two sets

FIG. 3. Bright field TEM image of $(Ba_{0.85}Ca_{0.15}O)_{1.02}TiO_2$.

TABLE 1. Results of ALCHEMI Determination

Specimen	C_x(%)	n
$(Ba_{0.85}Ca_{0.15}O)_{0.98}TiO_2$	9.0 ± 9.7	10
$(Ba_{0.85}Ca_{0.15}O)_{1.02}TiO_2$	26.3 ± 13.2	18

n is the number of determinations. The uncertainty in the C_x value was calculated as described in the following section.

of data, however, it can be shown that the difference in C_x values is indeed "significant" (for a 95% confidence limit), and cannot be accounted for by the spread in the data alone. Thus, it can be concluded that for the A site excess specimen, a definite fraction of calcium atoms is occupying Ti sites.

DISCUSSION

The ALCHEMI results show good qualitative agreement with the predictions of the equilibrium conductivity data, namely that a larger fraction of Ca atoms occupy Ti sites in the A site excess sample. Quantitatively, however, the ALCHEMI data appear to be less satisfactory. Assuming that for the A site excess sample, whose composition can be expressed as $(Ba_{0.867}Ca_{0.133})TiO_3 + 0.02\ CaO$, the excess CaO is distributed evenly among the Ba and Ti sites, thus:

$$0.02\ CaO \rightarrow 0.01\ Ca_{Ba}^{x} + 0.01\ Ca_{Ti}^{''} + 0.02\ O_{o}^{x} + 0.01\ V_{o}^{\bullet\bullet} \qquad (2)$$

the fraction of Ca atoms on Ti atoms sites (C_x) can be calculated to be 6.54%. This value may be compared with the value of 26.3 ± 13.2% obtained using the ALCHEMI technique. We now follow with a discussion of the errors involved in the ALCHEMI procedure.

X-ray production is a statistical process, so that even under ideal conditions, the number of counts in a given peak for a large number of trials will lie on a Gaussian curve [5]. Let $\bar{N}$ be the most probable value of the number of counts, then the standard deviation (σ) of the curve is given by $\bar{N}^{\frac{1}{2}}$. 95% of the readings will lie within 2σ of the mean, so that for a given determination of the number of counts N, the uncertainty is given by

$$\pm 2\sigma = \pm 2N^{\frac{1}{2}} \qquad (3)$$

Expressed as a relative uncertainty (%), this gives

$$\frac{2N^{\frac{1}{2}}}{N} \times 100\% \qquad (4)$$

Thus the lower the value of N, the higher is the relative error, so that >10000 counts are required to keep the error below ±2%. To see how this affects the ALCHEMI determination, it is useful to consider a particular example. In a given spectra, the number of counts in the calcium peak (N_{Ca}) will be significantly lower than in the barium and titanium peaks, thus for simplicity, we can assume that the error in N_{Ca} will be the largest contribution to the error in C_x.

The following table shows the actual number of X-ray counts for each element for an individual determination. The error in N_{Ca} is calculated from eqn. (3).

TABLE II.

Orientation	N_{Ba}	N_{Ti}	N_{Ca}
S-	53066	58426	7256 ± 170
S+	56734	73305	3068 ± 180

Substituting these values of N_{Ca} into eqn. (1) gives a maximum possible value of C_x of 45.8% and a minimum value of -3.9%. Fortunately, the uncertainty for a large number of readings is considerably less, and is given by

$$\pm \frac{t_{95}^{n-1}}{\sqrt{n}} \qquad (5)$$

where σ is the standard deviation for n determinations, and t_{95}^{n-1} is the student t value at the 95% confidence level.

Clearly the accuracy in C_X can be improved by increasing N_{Ca}, i.e., counting for longer times. However, errors due to specimen drift and contamination become more significant for long acquire times, thus a compromise must be made. Because the calculation of C_X is highly sensitive to the number of X-ray counts from the dopant element, the technique is limited to compositions in which sufficient counts can be obtained in reasonable times. Otherwise it becomes impossible to distinguish whether a change in the number of counts is due to channeling or statistical fluctuations.

The strength of the channeling effect which can be obtained is also an important factor, and this is dependent on the crystal structure and chemical composition [6]. The channeling which can be obtained in $BaTiO_3$ is relatively weak (~30% increase in the N_{Ti}/N_{Ba} ratio for the two orientations), hence the sensitivity of the C_X value to the count rate. Clearly for materials where the channeling is more pronounced, the accuracy will be improved.

CONCLUSIONS

The technique of ALCHEMI was used to determine the fraction of Ca atoms on Ti atom sites in Ca-doped $BaTiO_3$. The fractions were determined to be 9.0 ± 9.7% and 26.3 ± 13.2% for A site deficient ((Ba + Ca)/Ti = 0.98)) and A site excess ((Ba + Ca)/Ti = 1.02)) samples, respectively. The findings were consistent with the results of recent equilibrium conductivity studies which suggest that Ca can occupy Ti sites in $BaTiO_3$ and act as a doubly charged acceptor (Ca_{Ti}'').

ACKNOWLEDGEMENTS

We are grateful to Dr. J. Spence and Dr. J. Tafto for advice and helpful discussions. Financial support from the Office of Naval Research under contract number N00014-83-K-0190 is also gratefully acknowledged.

REFERENCES

1a. J.C.H. Spence and J. Taftø, Scanning Electron Microscopy, Vol. II, SEM Inc., 523-531 (1982).
1b. J.C.H. Spence and J. Tafto, J. Micros. 130, 147-154 (1983).
2. J. Appleby, Y.H. Han and D.M. Smyth, 85th Ann. Meeting of the American Ceramic Society, Chicago, April 25, Abstract 13-E-83 (1983).
3. M. Lal, M.P. Harmer and D.M. Smyth, to be presented at the 86th Ann. Meeting of the American Ceramic Society, Pittsburgh, May 1984.
4. N.H. Chan, R.K. Sharma and D.M. Smyth, J. Electrochem. Soc. 128, 1762-1769 (1981).
5. A.D. Romig, Jr. and J.I. Goldstein, Met. Trans A. 11A, 1151 (1980).
6. J. Tafto, Z. Naturforsch 34a, 452 (1979).

END

FILMED

3-85

DTIC